

This is to certify that the thesis entitled

POSITION, FORCE, AND PRESSURE MEASURES OF THE BODY IN VARIOUS CYCLING POSTURES

presented by

Chisom S. Wilson

has been accepted towards fulfillment of the requirements for the

MS ____ degree in ____ Mechanical Engineering___

Major Professor's Signature

Date

MSU is an Affirmative Action/Equal Opportunity Institution

LIBRARY Michigan State University

PLACE IN RETURN BOX to remove this checkout from your record. TO AVOID FINES return on or before date due. MAY BE RECALLED with earlier due date if requested.

DATE DUE	DATE DUE	DATE DUE
	<u> </u>	

2/05 p:/CIRC/DateDue.indd-p.1

POSITION, FORCE, AND PRESSURE MEASURES OF THE BODY IN VARIOUS CYCLING POSTURES

Ву

Chisom S. Wilson

A THESIS

Submitted to
Michigan State University
in partial fulfillment of the requirements
for the degree of

MASTER OF SCIENCE

Department of Mechanical Engineering

2006

Abstract

POSITION, FORCE, AND PRESSURE MEASURES OF THE BODY IN VARIOUS CYCLING POSTURES

By

Chisom S. Wilson

Non-traumatic injuries specific to bicyclists may be linked to forces present at the interfaces between the cycle and rider. These injuries include weakness and numbness of the hands and wrists, soreness of the pelvis, skin problems in the groin, erectile dysfunction and impotence.

The first goal of this investigation was to measure the forces present at the rider/cycle interfaces. Vertical and shear loads were measured for ten (10) subjects in a common fit position. The crank arm angles at which the maximum and minimum forces occurred were also obtained using a motion analysis system, and regions of rider contact with the seat were visualized with a pressure mapping system.

The second goal was to determine the effects of different hand positions on measured interface forces. Vertical and shear loads were measured after moving the handlebars 5cm closer to, then 5 cm further from the subject. A statistical analysis was performed using the SAS Mixed procedure with a significance level $\alpha = 0.05$. Several forces were significantly affected by changing the cycle's handlebar position.

Vertical loads were greater than shear loads, and in combination they may be contributing factors in non-traumatic injuries at the groin and hands reported by bicyclists.

Copyright by

Chisom S. Wilson

2006

Dedication

I would like to dedicate this thesis to my wife Jennifer, and to my family, Johnny, Sandra, Chelsea, and Chesney Wilson. Your belief in me instilled the dedication and confidence necessary to complete this work.

Acknowledgments

I would like to thank my advisor Dr. Tamara Reid Bush for her advice, ideas, and patience throughout the development and completion of this investigation. I would also like to thank my committee members Drs. Robert Hubbard and Dahsin Liu for their support, input, and suggestions.

To Dr. Joseph Vorro, your clarifying of the anatomy of the human body was immensely helpful.

Finally, I would like to thank Aaron Huber, Thomas Schneider, Cleveland
Thrasher, Nathan Remsberg, Jennifer Langridge, and Bethany Danielski. I would not
have gotten through this without all of your help.

TABLE OF CONTENTS

LIST OF TABLES	viii
LIST OF FIGURES	xii
Introduction and Literature Review	1
Bicycling Related Injuries	1
Engineering Perspective	4
Bicycling Posture	6
Scope of Research	8
Methods	10
Test Equipment	10
Experimental Stationary Bicycle	10
Load Cells	13
Motion Capture	14
Pressure System	16
Subject Recruitment and Selection	17
Testing	19
Subject Targeting	19
Equipment Preparation	24
Initial Device Setup	27
Test Descriptions	28
Measure of Ischial Tuberosities	28
Cycling Tests	28

Analysis	31
Results	37
Pedal and Crank Tangent Forces	39
Seat Vertical Forces	49
Forward/Rearward Seat Forces	56
Lateral Seat Forces	62
Seat Pressure Mapping	67
Handlebar Vertical Forces	69
Handlebar Forward/Rearward Forces	74
Handlebar Lateral Forces	80
Significant Effects due to Changes in Handlebar Position	86
Pedal Measures	86
Seat Measures	88
Handlebar Measures	93
Discussion and Conclusions	97
Baseline Rider/Cycle Interface Seat and Handlebar Forces	97
Seat Forces	97
Handlebar Forces	101
Timing Angles	102
Significant Effects from Changes to Handlebar Position	104
Pedal Data Comparisons	106
References	110

LIST OF TABLES

Table 1: Male Subject Anthropometry	18
Table 2: Subject Targeting Table	21
Table 3: Average Pedal Force Component Tangent to Crank Arm Path	42
Table 4: Angle at which the Applied Maximum and Minimum Force Compone to the Left Crank Arm Path Occurred (Timing Angle)	
Table 5: Lateral (side to side) Right and Left Pedal Maximum Forces;	44
Table 6: Timing Angle of Maximum Lateral Pedal Force	45
Table 7: Minimum Right and Left Pedal Lateral Forces;	46
Table 8: Timing Angle of Minimum Lateral Pedal Forces	47
Table 9: Range between Maximum and Minimum Lateral Pedal Forces	48
Table 10: Maximum Seat Vertical Force and Standard Deviation (SD)	50
Table 11: Timing Angles at which the Maximum Vertical Seat Forces Occurre	d50
Table 12: Minimum Seat Vertical Force and Standard Deviation (SD)	52
Table 13: Timing Angle of Minimum Seat Vertical Forces	53
Table 14: Range between the Maximum and Minimum Vertical Seat Forces	55

Table 15: Maximum Forward/Rearward (FR) Seat Force	57
Table 16: Maximum Forward/Rearward Seat Force Timing Angles	58
Table 17: Minimum FR Seat Shear Forces;	59
Table 18: Range between the Maximum and Minimum FR Seat Forces	61
Table 19: Maximum Lateral Seat Forces;	65
Table 20: Lateral Seat Force Timing Angles	66
Table 21: Range of Maximum Lateral Seat Forces	66
Table 22: Maximum Handlebar Vertical Force;	69
Table 23: Timing Angle of the Maximum Vertical Handlebar Force	70
Table 24: Minimum Handlebar Vertical Force	72
Table 25: Timing Angle of the Minimum Vertical Handlebar Load	73
Table 26: Range between the Maximum and Minimum Vertical Handlebar Forces	74
Table 27: Maximum FR Handlebar Forces	75
Table 28: Timing Angle of the Maximum FR Handlebar Force	76
Table 29: Minimum FR Handlebar Forces;	78
Table 30: Minimum Handlebar FR Force Timing Angles	7 9
Table 31: Range between the Maximum and Minimum FR Handlebar Forces	80

Table 32: Maximum Lateral Handlebar Forces	81
Table 33: Maximum Handlebar Lateral Force Timing Angles	82
Table 34: Minimum Lateral Handlebar Forces	83
Table 35: Minimum Lateral Handlebar Force Timing Angles	84
Table 36: Range between the Magnitude of the Maximum and Minimum	85
Table 37: Mean Pedal Forces That Showed a Statistically Significant Difference at	87
Table 38: Probability of Zero Difference in Pedal Forces	87
Table 39: Pedal Force Timing Angles That Showed a Statistically Significant Difference of P < 0.15 for at Least One Handlebar Position Change, i.e. Close-Far, Close-Regular, or Far-Regular	
Table 40: Probability of Zero Difference in Pedal Force Timing Angles	88
Table 41: Mean Seat Forces That Showed a Statistically Significant Difference at	89
Table 42: Mean Seat Forces in %BW that showed a Statistically Significant Difference $P < 0.15$ for at Least One Handlebar Change, i.e. Close-Far, Close-Regular, or Far-Regular	-
Table 43: Probability of Zero Difference in Seat Forces	91
Table 44: Mean Seat Force Timing Angles That Showed a Statistically Significant Difference of P < 0.15 for at Least One Handlebar Position Change, i.e. Close-Far Close-Regular, or Far-Regular	
Table 45: Probability of Zero Difference in Seat Force Timing Angles	92
Table 46: Mean Handlebar Forces That Showed a Statistically Significant Difference at P<0.15 for at Least One Handlebar Position Change	t .93

Table 47: Mean Handlebar Forces in %BW that Showed a Statistically Significant Difference of $P < 0.15$ for at Least One Handlebar Change, i.e. Close-Far, Close-	
Regular, or Far-Regular	94
Table 48: Probability of Zero Difference in Handlebar Forces	95
Table 49: Mean Handlebar Force Timing Angles That Showed a Statistically Signification Difference of P < 0.15 for at Least One Handlebar Position Change, i.e. Close-Facular, or Far-Regular	ır,
Table 50: Probability of Zero Difference in Handlebar Force Timing Angles	96

LIST OF FIGURES

Figure 1: Cyclist Positioned to Obscure the Axle of the Front Wheel with the Top of the Handlebars
Figure 2: Stationary Cycling Apparatus
Figure 3: Cycle crank arm and pedal surface
Figure 4: Anterior Target Locations http://members.aol.com/Attic21/Anatomy/skeleton1.html (8/21/2006)
Figure 5: Posterior Target Locations
Figure 6: Left Pedal Spindle and Back Pedal Targets
Figure 7: Cycle Seat and Load cell
Figure 8: Cycle Seat Height Adjustment
Figure 9: Laboratory (Global) Coordinate System;
Figure 10: Example of a Coordinate System Transformation from Unprimed to Primed Coordinates
Figure 11: Vector Describing the Left Pedal's Surface Orientation that was Used to Rotate the Left Pedal Forces into the Laboratory Coordinates; X'-axis into the paper
Figure 12: Definition of the Radial and Tangent Crank Arm Directions, as well as the Crank Arm Angle as Viewed from the Left Side of the Cycle
Figure 13: Work and Power Done by Pedal Forces

Figure 14: Profile of the Left Pedal Force Tangent to the Crank Arm Path; Single trial, single subject
Figure 15: Positive and Negative Work on Pedal
Figure 16: Vertical Seat Force Profile over Five Crank Arm Revolutions;49
Figure 17: Maximum Vertical Seat Force Timing Angle Histogram
Figure 18: Minimum Seat Vertical Force Timing Angle Frequency54
Figure 19: Forward/Rearward (FR) Seat Force Profile over Five Subsequent Crank Arm Revolutions; Single trial for one subject
Figure 20: Histogram of Minimum FR Seat Force Timing Angles
Figure 21: "Double Hump" Lateral Seat Force Profile;
Figure 22: "Single Hump" Lateral Seat Force Profile;
Figure 23: Top View of Seat Pressure Maps; Regions of greatest contact (pressure > 3.1 N/cm ²) at the maximum vertical seat force while the left leg was driving
Figure 24: Seat Pressure Map; Timing of the maximum FR and lateral seat forces. Grey regions indicated the greatest contact areas between the seat and rider (>3.1 N/cm²)
Figure 25: Handlebar Vertical Force Profile; Single subject
Figure 26: Frequency of Right Maximum Vertical and FR Handlebar Timing Angles 77
Figure 27: Representative Crank Torque Profile for One Crank Revolution in a Single Subject; Smak et al. (1999), Figure 1(a)

Introduction and Literature Review

Bicycling Related Injuries

For millions of people worldwide bicycle riding is a popular activity, enjoyed as a means of transportation, recreation, exercise, and sport. The health benefits of physical activity, including bicycling, have been well examined and documented. Moderate physical activity may lead to a reduced risk of premature mortality, heart disease, and diabetes (National Center for Health Statistics 2005).

Along with the health benefits, risks associated with bicycling and include both traumatic and non-traumatic injuries. Traumatic injuries to the head, skin, and limbs may occur from accidents such as falling off the bicycle and collisions with other cyclists, pedestrians, or motor vehicles. These injuries of bicyclists are typically treated through clinically standard treatments of traumatic injuries, as described in trauma literature (Mellion 1996).

Non-traumatic injuries associated with bicycling are also common and generally more clinically challenging to diagnose. These may include skin irritation and various musculoskeletal pains, with physicians attributing them to incorrect positioning, incorrect mechanics, and/or overuse (Mellion 1996, Weiss 1994).

Assuming that incorrect mechanics plays a role in non-traumatic injury, engineering research in bicycling biomechanics may help bridge the gap between simply studying "what hurts and where" and correction of the mechanics as viewed from a clinical standpoint. For example, biomechanics research has been helpful in elucidating the knee joint loads generated while riding a bike (Gregersen and Hull 2003) and

revealing potential mechanics anomalies in those bicyclists experiencing overuse knee injuries (Bailey et al. 2003).

Over the last several years there has been an increased interest in non-traumatic cycling related injuries specific to the interfaces of the bicycle and rider. Weakness and numbness in the hands and wrists, burning of the feet, soreness of the pelvis and ischial tuberosities (ITs), and skin problems of the groin that include bruising, chafing, boils, or ulceration (Weiss 1985, Andersen and Bovim1997) have been reported in recreational bicyclists. The development of perineal nodular indurations, or "accessory testicles," in the groin of elite and professional racing cyclists has also been reported (Vuong et al 1988, Kohler et al. 2000). Vuong et al. (1988) found these nodules to be pseudocysts that formed along the medial (inner) side of the ischial tuberosities of the pelvis, and were attributed to the repeated micro-trauma of the stretched fascia in the perineum during cycling. Necrotic (dead) tissue was also found around the edges of these indurations. Of all of the contact points, non-traumatic skin injuries at the rider/seat interface are the most frequently reported and discussed (Weiss 1994, Mellion 1996).

These injuries indicate tissue degeneration through compression and shear loading (stress), deformation (strain), and eventual breakdown during prolonged cycling activity. Extrinsic factors including pressure (Kohler et al. 2000), shear, temperature, and moisture (Weiss 1994) have been attributed to cause these injuries, and are similar to factors thought responsible in the development of decubitous ulcers (also called "pressure" sores) in the disabled (Hobson 1992, Edsberg et al. 1999, Bennet et al. 1979). Normal forces have been shown to be primary in reducing arterial blood flow to the skin of the

palm, but normal force magnitudes necessary to occlude blood flow were halved when combined with shear loading (Bennet et al. 1979).

Andersen and Bovim (1997) reported that 32 out of 160 (19%) respondent male participants in a long distance (540km) bicycle tour experienced weakness in the hands, while 67 (40%) reported numbness or "pins and needles" (paresthesias) in the hands and wrists. During the same bicycle tour, 33 (21%) of the male respondents reported numbness of the genitals, primarily on the penis. In an earlier and similar report by Weiss (1985), 12 out of 113 (11%) male and female respondents reported specific groin problems and of those, 81% reported numbness or paresthesias. Significant hand problems were also reported by about 10% of the survey respondents. From a study of 463 cyclists competing in at least one 320 km cycling event, Dettori et al. (2004) reported groin numbness by 31% of their respondents.

Potentially a more serious groin injury, epidemiological surveys have reported instances of male erectile dysfunction (ED) and impotence (inability to achieve an erection) in men who ride bicycles. Andersen and Bovim (1997) found that 21 of their 160 respondents (13%) reported impotence, and Dettori et al. (2004) reported that 4.2% of the respondents suffered ED at least one week after a long distance ride, while 1.8% continued to suffer after at least one month. They found ED to be strongly associated with groin numbness even though all were free of ED before the event. Groin numbness and/or pain may or may not be present with ED and impotence.

The underlying mechanisms of male groin numbness and ED may be a combination of nerve and blood flow problems, as they are sometimes present together in bundles. Nerve entrapment has been indicated as a possible culprit leading to decreased

sensitivity and a feeling of numbness in both the hands/wrists (Capitani and Beer 2002, Richmond 1994) and genitalia (Andersen and Bovim 1997, Weiss 1994). Riding a bicycle with traditional seat shapes have shown a reduction of the normal blood flow characteristics, and may have resulted from arterial occlusion during times of increased pressure on the groin while on a bicycle seat (Lowe et al. 2004, Munarriz et al. 2005, Nayal et al.1999). As such, bicycle seat designs have been modified to include extra padding, as well as cutout areas to reduce compression on the groin/perineum. Breda et al. (2005) showed that cyclists using a specific cutout saddle (Selle SMP) maintained higher levels of transcutaneous (on the surface of the skin) penile oxygen saturation compared to those on a traditional seat, which was an indicator of increased blood flow.

Interestingly, these seat designs may not minimize the incidence of ED or impotence. Cyclists using padded seats have reported more symptoms of irritation to the buttocks (Weiss 1985). Also, Dettori et al. (2004) found that men riding cutout saddles, which were designed to relieve pressure on the groin (and specifically the perineum), showed a slightly higher risk for ED alone, as well as increased risk for the combination of groin numbness and ED together. They also found a continued relationship between cutouts and ED even when considering those that reported pre-ride numbness. Riding a bicycle with the handlebars even with or higher than the seat also increased risk of ED, possibly indicating that the higher riding position relieved the hands and loaded the buttocks more.

Engineering Perspective

As with many seating related studies, from an engineering perspective bicycling studies have typically used some measure of interface pressure to characterize loading at

the interfaces. Pressure data have been evaluated using peak and mean surface pressures on different bicycle seats (Lowe et al. 2004) and in different hand positions (Bressel and Cronin 2004). Shear loading has been mentioned as playing a possible role in skin injuries (Hobson 1992, Edsberg et al.1999, Weiss 1994) but quantitative data has rarely been reported at the interface of the seat and rider, and to our knowledge not in the context as a potential tissue injury mechanism for bicyclists.

It has been shown that skin tissue over bony prominences previously subjected to pressure exhibits a subsequent change in its tensile mechanical properties (Edsberg et al. 1999) and it may be reasonable to assume a similar effect holds true for the skins shear properties. Skin over bone has also shown a lower tolerance to locally applied pressure in terms of reducing transcutaneous (on the surface of the skin) partial pressure oxygen measurements (Sangeorzan et al. 1989), as tissue pressure levels below the skin (subcutaneous) increased more rapidly than when skin is loaded over muscle.

Measurement of the interaction forces present at the interfaces of the bicycle and rider are limited to three studies accessible to this author. Bolourchi and Hull (1985) measured one force component at the seat, three at the pedals, and two at the handlebars in three subjects. They noted that at the time they were unaware of any other data of this kind, and indicated their research to be important in bicycle component design, as well as furthering knowledge of the biomechanical analysis of the pedaling process by collecting data across different pedaling frequency values. They reported "typical" data for one subject only and calculated the forward/rearward shearing force from an energy balance assuming symmetry from the right to left pedals and handlebars, but suggested this load should be measured in any future work.

Stone and Hull (1995) reported three force components at the seat, two at the handlebars, and three at the pedals, and attempted to find a linear relationship between a rider's weight and the maximum rider induced interface loads, again in the interest of frame and component design to obtain minimum weight and acceptable reliability. Five subjects were tested on a bicycle that was adjusted closely to their individual setups.

Stone and Hull (1995) found a strong correlation between the in-plane seat loads (forward/rearward and vertical) and body weight.

It is interesting that although the studies above reported that these load components were important to frame and component design, equivalent forces must also be resisted somewhere within a bicyclist's body tissues.

Bicycling Posture

Much work has been done on the biomechanical aspects of cycling and performance, especially with respect to "correct" positioning (posture) in terms of seat height above the pedals, to gain maximum benefit of the muscular power developed in the lower limbs and back. Research has dealt with the effects on pedal loading resulting from prolonged cycling (Sanderson and Black 2003), as well as the effects of seat height on oxygen consumption (Nordeen-Snyder 1977). The power curve generated during a cycle of each leg shows a region of both positive and negative contributions to the average driving power produced (Neptune and Herzog 1999), and efficient pedaling cadence frequencies have been optimized with regards to energy consumed (Foss and Hallen 2005).

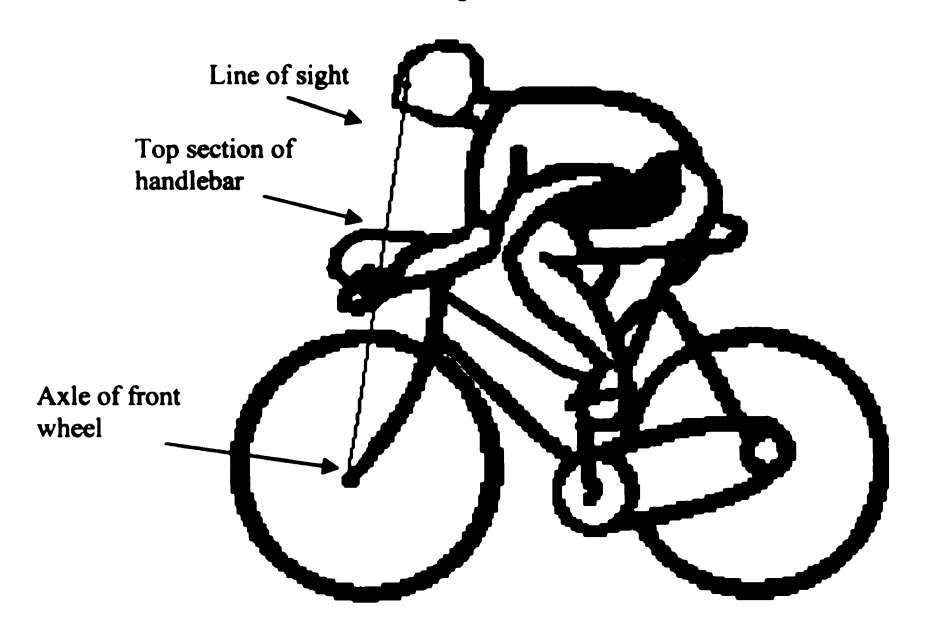
There exist little more than suggestions on the "correct" reach or "posture length" (de Vey Mestdagh 1998) from the seat to handlebars, and recommended methods are

based solely on anthropometrical relations. For example, one method suggests that when placing the elbow at the tip of the seat, a correct reach to the handlebar will cause tip of middle finger to bisect the center of lateral portion of the handlebar (Richmond 1994). This method was the starting point of a qualitatively assessed comfort survey by Christians and Bremmer (1998), and to our knowledge no quantitative data exist that report handlebar and seat loading in various postures defined by the reach from the seat to handlebars. De Vey Mestdagh (1998) pointed out, "... no matter what cycling posture is adopted, the upper body is used in an unusual manner." He then presented tabular data for "posture length" from the back of the seat to the handlebars based on a combination of the arm and torso length. These recommendations appeared to be based on visual observations of racing cyclists.

In commercially built bicycles, an appropriate frame size provides the rider with approximately one to two inches of clearance from the crotch to the top of the frame when straddling the bicycle in bare feet. Correct seat height above the pedals is then fine tuned with an adjustable seat post. The length of the frame is scaled with its height, so adjustments in the reach to and height of the handlebars, relative to the seat, are provided through different stem lengths (Mellion 1996). Setting the correct reach is important for correct distribution of the body weight between the front and back wheels, and is important for maneuvering (Phinney and Carpenter 1992).

One commonly used method in bicycle shops for attaining an initial seat to handlebar length is to have the subject first place their hands in the lowest (drop) section of the handlebars, and in their line of sight through the top section of the handlebar the axle of the front wheel should be obscured (Figure 1). Stems of different lengths are then

Figure 1: Cyclist Positioned to Obscure the Axle of the Front Wheel with the Top of the Handlebars



fit to the frame to accomplish this task. This method for setting the "correct" reach to the handlebars was also recommended by Phinney and Carpenter (1992).

Ashe et al. (2003) reported that body posture, and specifically reach, affected the untrained cyclist's performance measures of maximum oxygen uptake and mechanical efficiency. A study of EMG activity (Bressel and Larson 2003) of the triceps brachii in different handlebar positions showed significant differences in muscle activation between the top and drop handlebar positions, possibly indicating a shift in the force system supported by the hands at the handlebars. Changes to the cycling posture affected through changes in the reach from the seat to the handlebars may relieve some of the reported non-traumatic injuries through a reduction in the forces.

Scope of Research

The first goal of this investigation was to establish baseline interface force values and crank arm angles when those forces occurred (timing angles) during the cycling

activity for cyclists fit using an approach used in commercial environments to adjust the handlebars to the correct reach from the seat. It is theorized that these forces may contribute to the occurrence and severity of non-traumatic injuries commonly reported in the groin and hands of bicyclists.

The second goal was to determine if changes in the seat to handlebar length would affect the interface forces at the seat and handlebars. As there is only a limited range of stem lengths available, adjustability of approximately 5cm in either direction of a factory-installed stem are the maximum adjustment before necessitating a change in frame size.

The third goal was to make comparisons with pedal force data presented by other authors. This would confirm the validity of the methodology and test equipment used for this work.

To our knowledge, this is the first reported attempt to measure all interface loads during bicycling in several postures induced by changing the distance from the handlebars to the seat.

Methods

Test Equipment

Experimental Stationary Bicycle

A custom measurement device was developed and built by modification of a commercially available bicycle with a "mixte", or women's style frame design. The bicycle was mounted into a Velodyne stationary cycling device to allow riding the standard bicycle indoors (Figure 2). The front wheel was removed and the forks clamped

Figure 2: Stationary Cycling Apparatus

into the Velodyne, making it unnecessary for the rider to maintain his or her balance to keep the bicycle upright. The Velodyne also clamped the axle of the rear wheel, and the tire ran on a metal roller assembly attached through a shaft to an electronically braked unit and a 20 lb. flywheel. The flywheel was used to simulate inertial characteristics comparable to actual cycling on the road, and the tire was inflated to approximately 0.621 N/mm² (90 PSI) for each test.

Mounting the bicycle into the Velodyne elevated its height approximately 15cm (6 in.) above the laboratory floor. Although the complete device was stable once assembled, the "mixte" bicycle frame was chosen as a safety precaution as it allowed subjects the option of stepping through the frame rather than throwing the leg around the back of the seat when mounting and dismounting the device. There were also added benefits as stepping through the frame reduced the risk of disrupting the connection cables for the data acquisition equipment. Modification of the bicycle did not change its core functionality of transforming rotational motion from the legs of the rider into translational motion of the rider and cycle.

To maintain adjustability for sized subjects, the device's seat allowed vertical movement to accommodate riders of different leg lengths, and the handlebars, or grips were modified to separate the loadings of the left and right hands. Importantly, the handlebars were modified to maintain a standard grip width of 42cm while they allowed fore/aft and vertical adjustment to accommodate subjects with different stem length and/or stem height requirements.

The bicycle's crank arm (Figure 3 below) is the lever for the transferring the applied driving force from the feet to the back wheel. In this case the original crank arms were utilized, and had a length of approximately 165mm from spindle to pedal, which

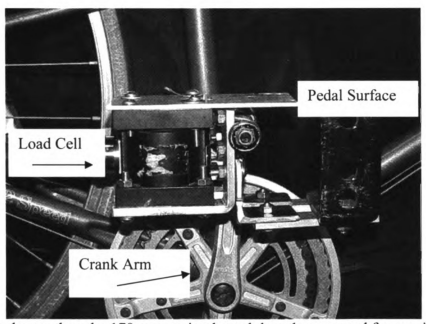


Figure 3: Cycle crank arm and pedal surface

was slightly shorter than the 170 mm optimal crank length suggested for maximum power output (Martin and Spirduso 2001). However, Martin and Spirduso (2001) found only a 4% difference in maximum power output across a crank length range of 120 – 220 mm in trained cyclists, which suggested our selection of crank arm length was adequate for this investigation.

The electronic display of the Velodyne provided continuous feedback to the subject, allowing him to maintain constant power output during cycling, independent of pedaling frequency (cadence), speed, and gear ratio. This feature was used during all tests so that each subject would maintain a constant power output of 125 watts, and created a

standard for qualitative and quantitative data comparisons both within and between subjects.

In conjunction with the Velodyne, a cycling computer (Cateye® Astrale 8) was fitted to the experimental cycle and indicated the subject's pedaling frequency (cadence) with a small magnet placed on the left crank arm and a magnetic pickup on the frame that sends a pulse to the cycling computer with each crank rotation.

Load Cells

To measure the forces present at the cycle/rider interfaces, five multi-axis force transducers (or load cells) were integrated into the bicycle between the frame and seat, frame and handlebars, and frame and pedals. In our experimental arrangement *all* forces and moments that resulted from the interaction between the subject and cycle acted through the load cells. Both pedals were instrumented independent of the other and similarly, as stated previously, the handlebars were modified and instrumented in such a way as to decouple the left and right sides. Each load cell was used to measure forces in three directions, Fx, Fy, and Fz, as well as three moments Mx, My, and Mz. Unlike the measured forces, which are only dependant on the direction of force application, the measured moments are dependant on the direction of applied force relative to a reference point; in this case the center of the force plate.

The load cells were Advanced Mechanical Technologies, Inc. (AMTI) MC3A series which were based on strain gage technology. Minimized gage cross talk between channels and thermal stability, through the use of four-arm bridges, are built into each load cell. Two 1,112 N (250lb) capacity load cells were located under the handlebar

grips, and 4,450 N (1000lb) capacity load cells were located under the seat and both pedals.

The load cells were mated with AMTI amplifiers and set to a gain of 1000. Each amplifier had a built-in filter for noise reduction, and all were set to 10.5 Hz for each test. A calibration file was incorporated for data acquisition and used the dominant diagonal calibration values provided by AMTI for each channel in the load cells. Although the load cells are precision instruments and their calibration values were factory measured. the load cell calibrations were checked once before and once after testing all subjects to assure validity. The pedal and handlebar load cells were removed from the bicycle, and known weights were applied in the vertical measurement direction. Known weights ranging from 111N to 445N (25lbf to 100lbf) were applied to the pedal load cells, and weights ranging from 22N to 89N (5lbf to 20lbf) were applied to the handlebar load cells. Due to the difficulty in attachment of the load cell under the seat, it was not removed for calibration. Instead, a board was placed across the top surface of the seat before known weights ranging from 222 N to 556N (50 lbf to 125 lbf) were applied. It was expected that the largest reaction forces would occur in the vertical direction to counteract the body force, and all five force plates showed accurate and repeatable calibration measurements for each of four known weight values both before and after testing.

Motion Capture

A Qualisys motion measurement system was utilized to track the positions of retro-reflective targets placed at key landmarks on both the subject's body and the experimental cycle. Five motion cameras positioned around the test area collected motion data at their maximum frequency of 60 Hz. Clusters of infra-red (IR) light

emitting diodes (LEDs) surrounded each camera lens. Each camera's image sensor detected the reflected IR light from the retro-reflective targets and returned two-dimensional position data. Three-dimensional position data was calculated through proprietary Qualisys software that required each retro-reflective target be seen at all times by at least two cameras. The use of IR reflection allowed for testing to be conducted under regular laboratory lighting conditions.

Retro-reflective targets were made from lightweight wooden spheres with a diameter of approximately 20mm attached to a flexible base similar to vinyl. The base was oblong in shape to provide a suitable surface for taping to the subject's skin. The spheres were completely covered with 3MTM high gain 7610 industrial grade reflective sheeting that provided 700-900 times more luminescence compared with light reflection from a white screen, even when viewed from significant angles. The fully coated, spherical shape of the targets helped maximize visibility in the various positions attained throughout testing.

The motion system was calibrated just prior to each subject's test, even when testing more than one subject per day. The calibration structure had four retro-reflective reference targets at known, fixed positions on a frame, as well as a wand of known length with retro-reflective targets at both ends. The static structure set the global coordinate system of the test area, while movement of the wand in the test space provided a method for calibrating a region of the lab larger than the frame itself. Together they provide a length scale for the tracking system. Linearization files provided by the manufacturer for each camera lens were loaded into the collection software prior to each calibration, as were the length parameters for the calibration structure and wand.

Pressure System

A Tekscan Body Pressure Measurement SystemTM (BPMS) was used primarily as a qualitative tool to determine where regions of contact occurred at the seat/rider interface. The BPMS collects interface pressure information with a pressure mat, a thin printed circuit encased in a flexible plastic backing material (~20"x17"x0.012"). The sensor (Tekscan Model #5315) was made up of 2,016 "sensels" arranged in a matrix of 48 columns and 42 rows across the mat. Each "sensel" varied resistance with a change in the average load applied across its surface and can detect pressures within a range of 0 - 0.0345 N/mm² (0-5 PSI) when properly calibrated.

Calibration of the BPMS required first that each pressure mat be conditioned, a process of repeatedly loading and unloading the mat with even pressure distribution.

Using a rubber bladder device developed by Tekscan, the entire sensing area of the mat was loaded evenly to approximately 0.0172 N/mm² (2.5 PSI) and held for 30 seconds.

The pressure was then released and the mat was allowed enough time to return to its initial state of near zero before another load/unload sequence. Two mats were used during this investigation and ten conditioning sequences were performed for each mat prior to its use.

After conditioned, the pressure mat was equilibrated under constant pressure of approximately 0.0172 N/mm² (2.5 PSI) over its entire surface using the previously described air bladder system. Equilibration effectively zeroes the pressure acquisition system across every "sensel" in the sensor's matrix. The equilibration file was then loaded into the computer software prior to calibration.

Calibration of the pressure system allowed for either a one point linear calibration (assuming a zero load after equilibration) or a non-linear calibration using two data points at different load levels. Tekscan recommended a calibration load of at least 80% of the maximum load expected to be seen for a one-point calibration. The pressure mat was placed on a hard surface (plywood) and 334 N (75 lbf) of dead weight were used to directly load the measurement area for the first data point. The hard surface was chosen to minimize any surface deformation of the mat due to the load placement. The maximum pressure saturation value was noted and next a 445 N (100 lbf) load was applied for the second data point and the maximum pressure saturation value was again noted. Although the pressure mat system was used primarily for qualitative analysis, the calibration file resulting in the highest saturation pressure resolution was used to increase the accuracy in pressure measurements. With a weight diameter of approximately 267 mm (10.5 inches), the loaded area of the mat was approximately 56,200 mm² (87 in²) and covered the area that would be loaded during testing.

Subject Recruitment and Selection

Results from this research may be applicable to any person who rides a bicycle and as such, subjects were initially recruited from the general population as well as from the avid cycling community for a pilot study. Potential subjects were brought into the laboratory and asked several questions pertaining to their cycling activities. Examples included age, number of years of cycling experience, most frequent type of cycling activity, and if they had recently experienced any type of internal (i.e. knee or groin) injury. Potential subjects under the age of 18, those who were pregnant, and those reporting an injury were dismissed as participants for this study (those who reported an

injury were not included because of the possibility of data variability due to such an injury).

After initial screening of potential subjects, the testing protocol was discussed with each qualified subject. If agreeable, he or she was asked to sign an approved consent form (MSU CRIRB #05-456) to be interviewed, tested, and photographed. Three males and one female subject participated in the pilot study, and within the male group one subject was an avid cyclist while the other two were not. The female subject was an experienced cyclist.

Data acquired from pilot testing indicated fluid movement patterns and smooth force curves for the avid cyclists of both genders. Also, a recent investigation by Bressel and Cronin (2004) showed significant differences in seat pressures between males and females in several different cycling positions. From these observations we decided to include only avid or recreational male cyclists as subjects for this investigation, and recruitment was done through the placement of fliers at several local bicycle shops. In total 12 male cyclists participated as test subjects for this research. Due to complications that arose in data collection with two of the subjects, data from ten were used in this analysis.

Table 1: Male Subject Anthropometry

Subject	Height	Weight	Activity
	cm (in)	kg (lbf)	Miles/Week
0	172.7 (68)	65.8 (145)	200
1	177.8 (70)	72.1 (159)	100
3	173.4 (68.25)	71.9 (158.4)	50
4	180.3 (71)	80.3 (177)	225
6	181.6 (71.5)	71.5 (157.6)	150
7	185.4 (73)	74.8 (164.8)	220
8	185.4 (73)	77.7 (171.2)	70
9	175.3 (69)	72.1 (159)	135
10	175.3 (69)	69.4 (153)	60

11	181.6 (71.5)	82.2 (181.2)	100
Max	185.4 (73)	82.2 (181.2)	225
Min	172.7 (68)	65.8 (145)	50
Ave	178.9 (70.4)	73.76 (162.6)	131
Std. Dev.	4.695 (1.848)	5.0221 (11.07)	65.9

Testing

Subject Targeting

Prior to a subject's arrival in the lab, gauze and alcohol swabs were readied to clean the subject's skin. The retro-reflective targets were laid out and a hypoallergenic, breathable medical tape used for fixation to the skin was applied to the target base. The adhesion between the target and its backing material was also checked to ensure dynamic stability of the target during testing.

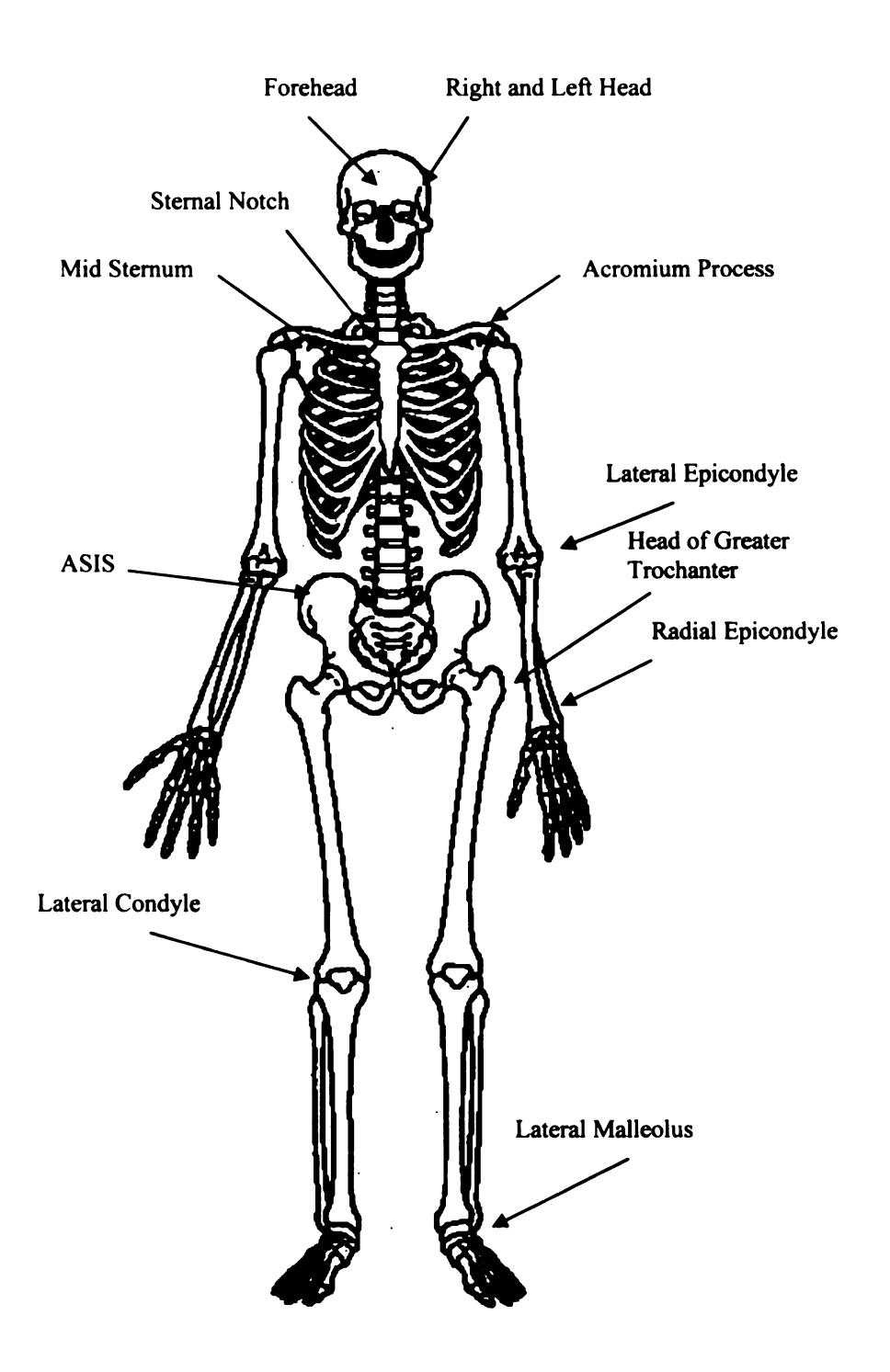
Once the subject was familiarized with the investigation and signed the consent form, he was asked to change into tight-fitting attire, including cycling shorts, a shirt, and athletic shoes. Clip-in style bicycle shoes and pedals were not used for this study. Nine of the ten subjects chose not to wear a shirt to improve the placement of back and chest targets directly on the skin. The subjects were then weighed without shoes or socks, and a measure of body fat was taken using the bioelectrical impedance method with a Tanita® TBF-551 Body Fat scale. The scale passes a very low electrical signal through the body and the subject's body fat percentage is returned based on impedance figures from the manufacturer's calibration.

The subject's inseam length was measured at this time without his shoes or socks. With his back to the wall, the subject was asked to hold a thick ruler firmly into his crotch. A bubble level was used to level the ruler with the floor and the inseam length was measured from the lab floor to the top of the ruler.

Next, the subject was seated and asked to put on his socks and athletic shoes to begin target placement. Targets were affixed bilaterally at various locations including bony prominences near the ends of the limbs. Table 2 contains a listing of targeted locations on the body. Anatomic locations of target placements can be seen in Figure 4 and Figure 5.

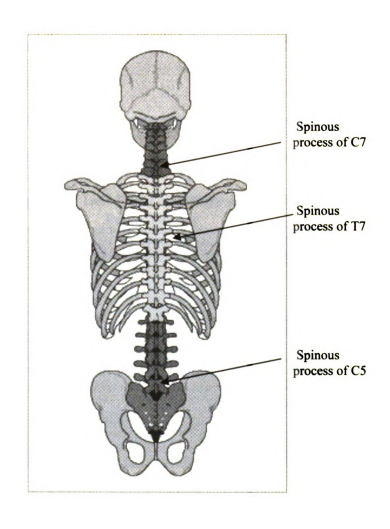
Table 2: Subject Targeting Table		
Sternal Notch		
Mid-sternum		
C7 (Spinous Process of the Seventh Cervical Vertebra)		
T7 (Spinous Process of the Seventh Thoracic Vertebra)		
L5 (Spinous process of the Fifth Lumbar Vertebra)		
Right and left side of head at approximate center of gravity (approximately over the inferior aspect of the joint between the sphenoid and temporal bones and 1 cm above the mid-line of the Frankfort plane)		
Forehead		
Right and left acromion process (shoulder)		
Right and left anterior superior iliac spine (ASIS)		
Right and left head of greater trochanter (Hip)		
Right and left mid-thigh		
Right and left lateral condyle (knee)		
Right and left mid-shank		
Right and left lateral malleolus (ankle)		
Right and left heel		
Right and left tip of second toe		
Right and left lateral humeral epicondyle (elbow)		
Right and left radial epicondyle (wrist)		

Figure 4: Anterior Target Locations http://members.aol.com/Attic21/Anatomy/skeleton1.html (8/21/2006)



22

Figure 5: Posterior Target Locations www.biorelax.hit/bg/posterior_spine.gif (8/22/06)



Once fully targeted, several basic anthropometric measures were taken. Link length measurements of the arms and legs were taken on all subjects along the right side of the body. The distance between the right and left acromium process was measured to determine the approximate width of the shoulders. The width, depth, and height of the pelvis were also measured.

Additionally, two targets were permanently affixed to the experimental cycle at the left pedal spindle and the back of the left pedal, Figure 6 below. The spindle target

Pedal Targets

Back Pedal Target

Target

Figure 6: Left Pedal -- Spindle and Back

was used to ascribe a reference frame for various events that occur during a single pedal stroke (0°-360°). As the pedal load cells are free to rotate about their spindles, the left-spindle and left-back pedal targets were used to assign a local coordinate system during data reduction for transformation of the local left pedal forces into global (laboratory) forces. There were no other targets placed on the eveling device.

Equipment Preparation

Calibration of the pressure and camera system was done before each subject's testing sequence began. The motion cameras, load cell amplifiers, and all computer systems (pressure, force, motion, and Velodyne) were turned on at least 15 minutes before calibration began to ensure that all components were properly warmed up.

Calibration of the pressure system was typically accomplished prior to the subject arrival in the lab and was carried out according to the previous description in the Test Equipment section.

Before calibrating the motion system the cycle device was unplugged and removed from the testing area, and care was taken to either cover or remove all reflective objects from the field of view of any camera. The motion calibration sequence was run twice according to the manufacturer's instructions to assure similar calibration values, and was captured at the maximum frame rate for the cameras (60 Hz) for ten seconds. The second calibration file was loaded into the motion capture software in preparation to begin testing.

After motion calibration, the cycle device was reintroduced into the test space. The load cell cables were reattached, and the pressure mat was placed on the seat surface. Each load cell's amplifier channels were balanced with the seat and handlebar mounts in place. The pedals were held such that the pedaling surface was parallel to the ground so that the only force acting on the transducer was from the aluminum pedal surface. Also, the handlebar mounts and seat surface were leveled with a bubble level to replicate their position during testing. An initial force file was taken at 60 Hz for two seconds. Since these initial force data values were already present before any testing began, they were subtracted off of all force files during later data reduction. With the seat's load cell in a fixed position relative to the seat surface (Figure 7), the correct "zeros" could be subtracted prior to transformation from local force coordinates into lab coordinates.

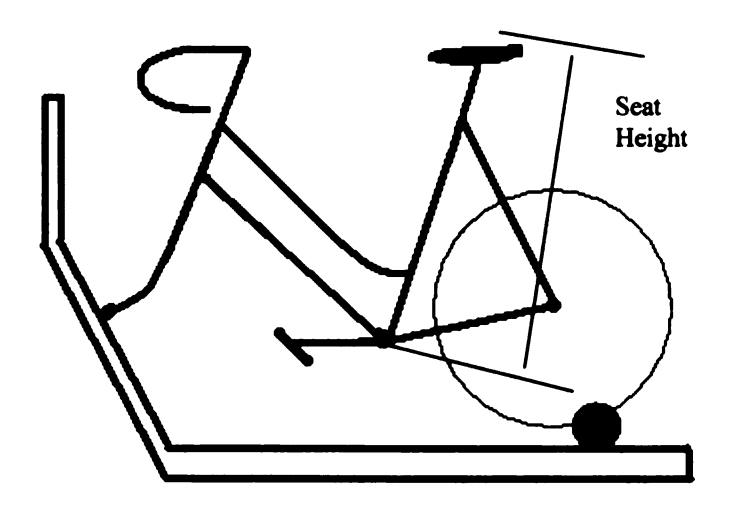
Figure 7: Cycle Seat and Load cell



Initial Device Setup

The cycling device's seat height was initially set according to each subject's seat height on their own bicycle, and was measured from the center of the crank arm spindle to the top of the seat surface directly above the center of the load cell. Small adjustments

Figure 8: Cycle Seat Height Adjustment



were made as requested to accommodate for small differences between the height of the pedaling surface and spindle on the device as compared to the subject's own bicycle pedals. The handlebar tops were then set approximately level with the seat surface, and the length from the seat to the handlebars was also adjusted to that of their own bicycle. Setting the handlebar tops level with the seat is a recommended starting point for cycling comfort (Mellion 1996), and is common in retail bicycle stores for initial fit adjustments on new bike purchases.

Test Descriptions

Measure of Ischial Tuberosities

A static pressure file was collected to approximate the width of the ischial tuberosities (ITs), or sit bones, as this is a difficult and sensitive area to accurately measure with an anthropometer. The stiff wooden platform used during pressure calibration and the calibrated pressure mats were left in the test area just prior to motion calibration. The subject was asked to sit on the mat with their back perpendicular to the platform, feet flat on the floor, and forearms resting along the knees. In this upright seated position it was relatively easy to discern the two highest areas of pressure concentration and estimate the location of the ITs. The subject was asked to hold this position and a pressure file was collected for five seconds at 60 Hz. No force or motion data were collected concurrently with this test.

The pressure mat was replaced onto the top of the seat, and the wooden platform was used to aid the subject in mounting the cycling device. The platform was subsequently removed before all other testing.

Cycling Tests

With the seat height adjusted according to the subjects own bicycle (see description of Initial Device Setup), the subject was asked to place his hands in the drop section of the handlebars and indicate if a handlebar adjustment was required in the fore and aft direction to obscure the axle of the Velodyne that clamped the front forks of the cycle. Reach adjustments and checks were continued until the subject indicated he could no longer see the front fork clamp in their line of sight through the top portion of the

handlebar. This was considered the Regular position and was the starting point for testing.

The subject began to pedal the cycle and warmed up in the Regular position for approximately 10 minutes with the external power output controlled at 100 watts, and a subject regulated pedaling frequency of 72-78 rotations per minute (RPM) via feedback provided by the cycling computer. This warm-up period allowed the subject to become familiar with the cycle set up, and gave them a feel for the desired pedaling frequency for each test.

After the warm-up period the external power output was increased on the Velodyne to the desired testing value of 125 watts. The subject was then asked to maintain a constant pedal frequency in the range of 72-78 RPM, with a desired frequency of 75 RPM. After an adaptation period of two minutes at the new workload, five seconds of motion, force, and pressure data was collected simultaneously at 60 Hz. Over the next one and a half minutes, two additional five second trials were collected.

For the next set of tests, the subject was asked to stop pedaling and move the right pedal and crank arm to the forward horizontal position. His foot was positioned such that the first metatarsal of the big toe lined up vertically over the spindle of the pedal and using a commercially available bicycle foot strap was strapped down to the pedal surface. The subject then rotated the left crank arm forward and the process was repeated for the left foot.

The subject was asked to begin pedaling again, and the power was increased to the desired 125 watts. Once the subject reached the desired steady state pedaling

frequency (~75 RPM), he was given a two-minute adaptation period and three sets of data were collected exactly as described above.

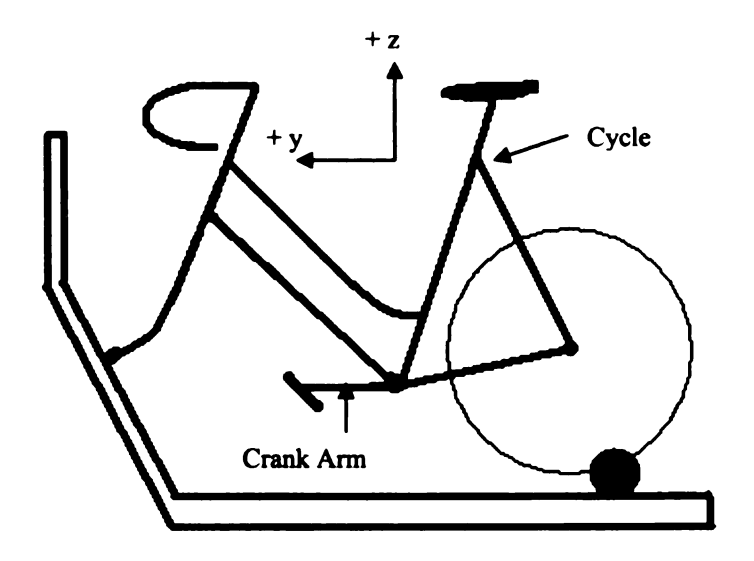
After accomplishing all pedaling tests in the Regular handlebar position, the power output was incremented down to 0 watts as the subject stopped pedaling. The handlebars were then moved closer to the seat by approximately 5 cm, defined as the Close position. The distance of 5 cm was chosen as it was expected that this would be on the extreme short end of the range of stem lengths commercially available for purchase. The testing procedure was repeated almost exactly as described for the Regular position, with the only exception being the sequence of strapping the feet to the pedals. At the end of the Regular position testing, the subject's feet were left strapped onto the pedals. These three sets of strapped data were collected first in the Close position. The subject's feet were then un-strapped, and again three sets of data collected.

Once all tests were complete in the Close handlebar position, the subject was asked to stop pedaling and the power output was incremented down to zero. The handlebars were then moved 10 cm forward of the Close handlebar position, or 5 cm forward of the initial Regular handlebar position, to the Far handlebar position. The distance of 5 cm forward of Regular was chosen to approximate the extreme far end of commercially available stem lengths that a person may select for personal use. Once adjusted to the Far position, testing was carried out exactly as described previously for the Regular position, as this time the subject's feet were un-strapped in the last test of the Close position.

Analysis

The laboratory coordinate system was defined during motion calibration with the +y-axis directed towards the front of the cycle, the +z-axis directed away from the lab floor, and the +x-axis directed to the right and away from the cycle, Figure 9. This

Figure 9: Laboratory (Global) Coordinate System; +x Axis Pointed Into Paper

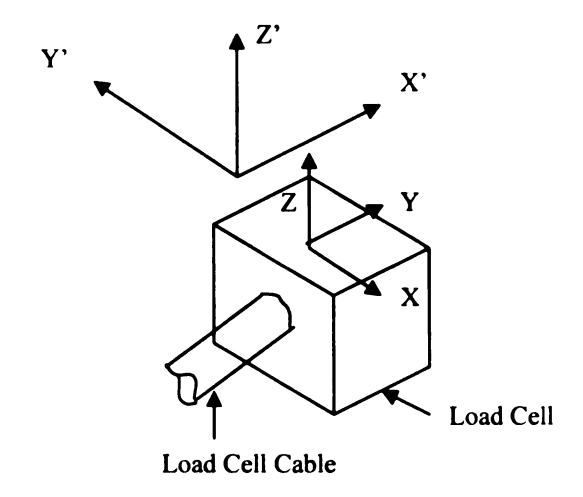


orientation was chosen to minimize the number of necessary coordinate transformations of the load cell data.

To assure that the load cell cables did not interfere with normal pedaling of the cycle, originally the load cells axes did not necessarily coincide with each other, or with the laboratory coordinate system. For example, the left handlebar and left pedal load cells were oriented with their cables exiting to the left of the cycle, while the right handlebar and pedal were oriented with their cables exiting the load cell to the right of the cycle.

It was desirable to describe all of the measured force data in the same coordinate system as the motion data, which necessitated coordinate transformations at all of the load cells. As an example, to arrive at the X' and Y' axes as shown in Figure 10, the

Figure 10: Example of a Coordinate System
Transformation from Unprimed to Primed Coordinates



forces measured in the X and Y directions of this load cell coordinate system were rotated by an angle of $\theta = 90^{\circ}$ about the Z-axis through the transformation matrix shown in Equation 1. The coordinate transformations were automated with a computer algorithm. This algorithm also subtracted any initial force data (zero file) from the raw

Equation 1: Transformation from unprimed to primed coordinate system; $\theta = 90^{\circ}$

$$\begin{pmatrix} FX' \\ FY' \\ FZ' \end{pmatrix} = \begin{bmatrix} \cos\theta & \sin\theta & 0 \\ -\sin\theta & \cos\theta & 0 \\ 0 & 0 & 1 \end{bmatrix} \begin{pmatrix} FX' \\ FY \\ FZ' \end{pmatrix}$$

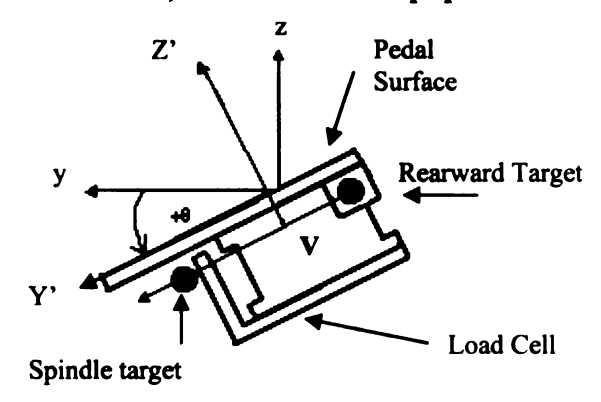
force data of each trial, performed the appropriate coordinate transformations corresponding to an individual load cells orientation, and output the corrected force data into a spreadsheet file. During pilot testing, several transformed values were checked via hand calculations to verify that the computer program worked properly.

Equation 2: Calculation of the pedal surface unit vector as the original vector divided by its magnitude

$$\hat{V} = \frac{V}{|V|}$$

A single coordinate transformation was adequate to attain force data from the handlebars and seat load cells that coincided with the motion data in the laboratory coordinates. However, the pedal load cells were unique, as they also rotated about their X'-axes while pedaling, Figure 11. Thus, an additional transformation was needed to

Figure 11: Vector Describing the Left Pedal's Surface Orientation that was Used to Rotate the Left Pedal Forces into the Laboratory Coordinates; X'-axis into the paper



fully describe the pedal forces in terms of the laboratory coordinate system. This was done after motion data was imported into the corrected force data spreadsheet file.

Recalled from the Methods section, the left pedal was targeted to find a vector parallel to the orientation of the pedal surface. This vector described the position of the pedal spindle target relative to the rearward pedal target (V in Figure 11) and was used to define the angular orientation of the pedal surface (Y'-axis) in the laboratory y-z plane. As V was described in laboratory y and z coordinates directly from the motion data, a unit vector (magnitude equal to 1) \hat{V} was calculated parallel to V.

Next, the laboratory y-axis was assigned a unit vector \hat{y} , and the angle θ was calculated as the arccosine of the component of the unit vector \hat{V} in the direction of \hat{y} , Equation 3. An orthogonal Z'-axis was subsequently defined normal to and directed

Equation 3: Calculation of the pedal surface angle relative to the laboratory coordinate system; V(y) was the y-component of the unit vector V

$$\theta = \arccos \left(\hat{V}(\hat{y})\right)$$

away from the pedal surface (see Figure 11). Finally, the force data from the left pedal's load cell was transformed into the laboratory coordinate system according to Equation 4.

The motion data from the left pedal spindle target was also used to ascribe a radial vector coinciding with the longitudinal neutral axis of the crank arm (Figure 12).

As the crank arm rotated in the y-z plane, the maximum and minimum y and z positions

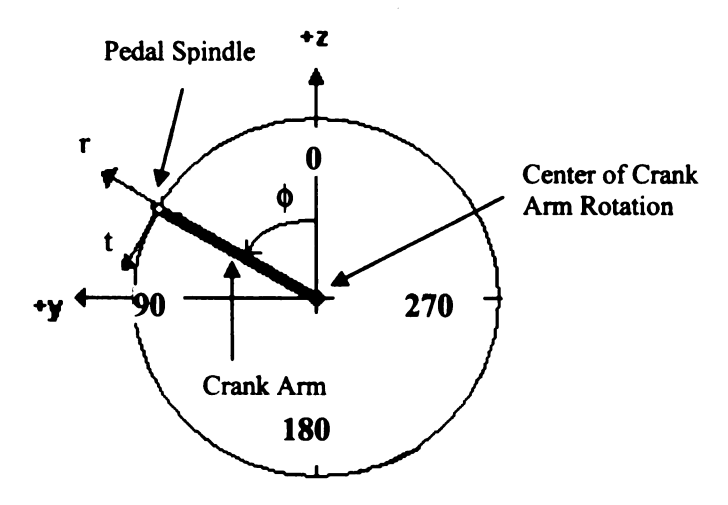
Equation 4: Additional pedal force transformation into laboratory coordinates

$$\begin{pmatrix} Fx \\ Fy \\ Fz \end{pmatrix} = \begin{bmatrix} 1 & 0 & 0 \\ 0 & \cos\theta & \sin\theta \\ 0 & -\sin\theta & \cos\theta \end{bmatrix} \begin{pmatrix} FX' \\ FY' \\ FZ' \end{pmatrix}$$

for the pedal spindle were found. These respective minimum and maximum values were averaged to obtain the y-z position for the center of crank arm rotation. A position vector was then calculated in laboratory y-z components from the calculated center of the crank arm rotation to the pedal spindle target describing the radial direction (\mathbf{r} , Figure 12) of the crank arm. The crank arm angle ϕ was found using a similar procedure to that described for the pedal surface angle represented by θ . The left crank arm angle was defined as 0° when it coincided with the laboratory z-axis, and subsequent crank arm angles were

positive in a counterclockwise movement as viewed from the left hand side of the cycle as seen in Figure 12.

Figure 12: Definition of the Radial and Tangent Crank Arm Directions, as well as the Crank Arm Angle as Viewed from the Left Side of the Cycle



The difference between the left pedal surface angle (θ) and crank arm angle (ϕ) was used to develop the force component used to drive the crank arm through a revolution; that which was tangent to the crank arm path. The tangent force component has been studied previously by other authors, and it was also calculated in this work as to allow comparisons with reported literature.

In each handlebar position (Close, Regular, and Far as described in the Methods section), two of the three trials were analyzed. The two trials were selected based on their completeness of force, motion, and pressure data. The force and motion data were cyclical in nature, and the maximum and minimum force values for each of five complete, continuous crank arm revolutions per trial were evaluated. The maximum and minimum forces were chosen since they represented the extreme force values that must be resisted somewhere within the subject's body. This method was previously used by Stone and Hull (1995) to determine if interface force values were correlated with a

subject's weight. Here, the maximum and minimum force values were also calculated as a percentage of the subject's body weight (% BW). Additionally, the left crank arm angles at which the maximum and minimum interface forces occurred were also retrieved from the motion data and defined as "timing angles." Mean (average) and standard deviation (SD) values of the ten maximum forces, ten minimum forces, forces in % BW, and ten timing angles for each handlebar position were then calculated and analyzed to arrive at a grand mean for all of the subjects tested.

Finally, it was hypothesized that a change in the reach, defined by the distance between the seat and the handlebars (i.e. Close, Regular, and Far), would not significantly affect the magnitudes of the forces present at each of the rider/cycle interfaces. Thus, a statistical analysis was done using the Mixed Procedure in SAS v9.1, which compared the mean maximum forces, minimum forces, and timing angles across the subjects in all three handlebar positions. With the confidence level set at 95%, significant differences in the force and timing angle values were present for *P* values less than 0.05.

Results

The quantified values presented in the tables and figures in this section were measured with all subjects set up in the Regular handlebar position, described previously in the section titled Research Methods. Due to the quantity of data collected, data from the Close and Far handlebar bar positions were used for statistical comparisons. Due to problems with data collection and storage, significant data loss occurred for subjects 2 and 5. Therefore, analyses for these subjects were not conducted.

Although the test protocol involved data collection both with and without the subject's feet strapped to pedals, only an analysis of the feet strapped to the pedals was presented here. During the early phases of data collection, several subjects voiced concern that their feet were slipping on the pedal surface when they were not strapped to the pedal, which made it more difficult to maintain a consistent and smooth pedaling cadence. Having the subject's feet strapped to the pedals also more accurately represented the realistic bicycling situation, as the trend for recreational and avid bicyclists is to have their shoes mechanically coupled to the pedal with either foot straps, or clip-in style pedals similar to ski bindings.

Force data collected from the pedals, seat, and both the left and right handlebars will be presented, as well as pressure mapping data collected from the seat. Mean (averaged) values of the maximum and minimum forces were computed over ten complete revolutions of the left crank arm, with the standard deviation (SD) included in parentheses. The force values were also calculated as a percentage of the subject's body weight and are included in tabular form. The pedal forces have been rigorously studied by other authors and were not the main focus of this investigation. Therefore, not all of

the pedal forces were analyzed, and those presented in this work were included to make comparisons with previous investigations.

To develop an understanding of when the maximum and minimum forces occurred during the pedal stroke, left crank arm angles corresponding to a maximum or minimum force were defined as a "timing angle." All timing angles were defined with 0° as the highest point of the left crank arm during a pedal revolution, and positive angles measured in a counterclockwise fashion as viewed from the left side of the cycle.

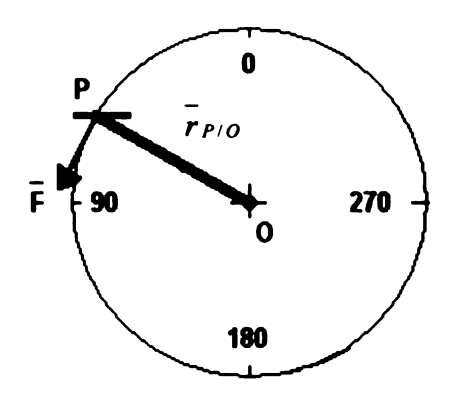
Finally, the results of a statistical analysis that described the effects of changing the reach to the handlebars on the forces will be presented. The statistical analysis was done for all of the presented values, but only those that indicated a significant difference existed in the force values for the different handlebar positions were included here. The quantification of statistical significance was reported for values of P < 0.15 with a confidence level set at 95%.

Pedal and Crank Tangent Forces

Force data was collected at both the left and right pedals. However, only the left pedal was targeted and the local pedal coordinate system was defined to calculate the relative angle between the pedal surface and the crank arm. The pedal forces were then transformed and gave a force vector with components described as parallel and perpendicular to the crank arm.

Work was done on the crank arm, and hence power delivered to drive the rear wheel of the cycle device, through the pedal force component perpendicular to the crank arm, Figure 13.

Figure 13: Work and Power Done by Pedal Forces



As a reminder, work done by forces on the pedal was the product of an applied force and the distance over which that force acts.

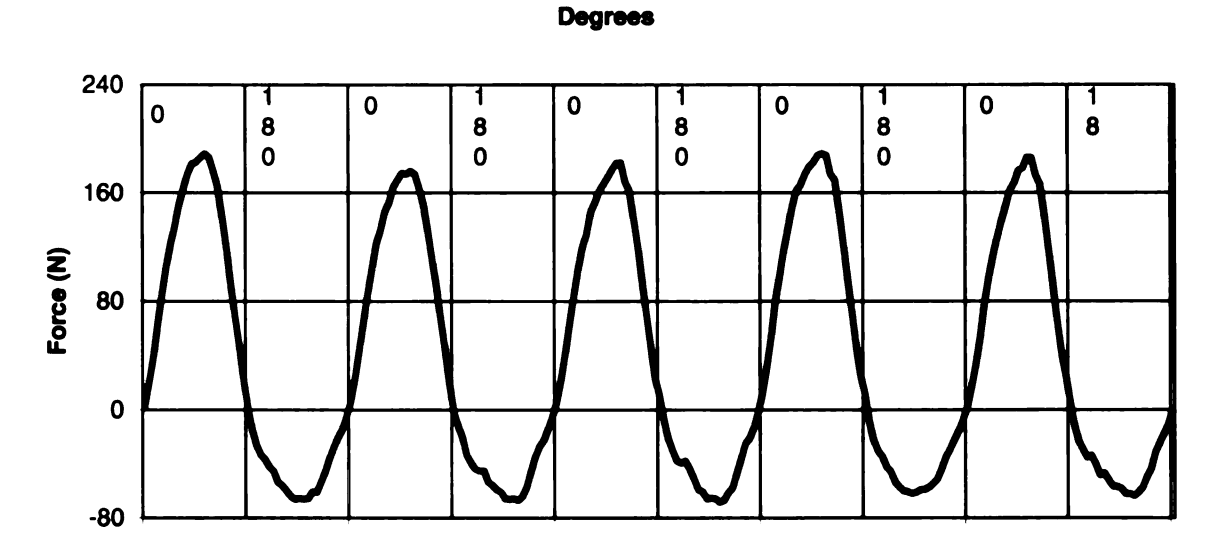
Work = Force x Distance

Power was then the total amount of work done over a period of time.

Power = Work / Time

In the case of the cycle, instantaneous power was the product of the force component tangent to the path of the crank arm (Figure 14) and the tangent component of the left pedal spindle velocity vector. These quantities were available through the load cell and motion data.

Figure 14: Profile of the Left Pedal Force Tangent to the Crank Arm Path; Single trial, single subject



Shown in Figure 15 below, the left pedal force component tangent to the crank arm path was positive in the region from 0-180°, provided positive work about the center

Positive Tangent Component Negative Tangent Component

Figure 15: Positive and Negative Work on Pedal

of the crank arm's path, and contributed positive power to drive the left crank arm. In the region approximated by 180-360° the force component of the left pedal was negative, and contributed work against the rotation of the crank arms. From this observation, the left leg was considered to be "driving" when its angular position moved through 0-180° and "non-driving" when its angular position moved through 180-360°. In the negative region, a portion of the positive work and power provided by the driving leg was used to overcome the negative work from the force applied through the non-driving leg.

Although force data was collected from the right pedal, a measure of the tangent force was not possible. Since the right pedal was not targeted no local coordinate system could be defined. It was assumed that the right pedal displayed a similar tangent force profile to that of the left pedal, and therefore the right leg was considered as "non-driving" during 0-180° and "driving" during 180-360° of the crank arm revolution.

For the left pedal, the maximum and minimum pedal force component tangent to the crank arm path varied across the subjects even with the average power output maintained at 125 watts for all tests. In the Regular position, the average maximum force values ranged from 143N (11N) for Subject 4 to 212N (8N) for Subject 11, with a grand mean of 173N (24N) across all of the subjects. The average minimum force ranged from -59N (6) to 103N (4N), with a grand mean of -84N (16N). The negative values associated with the minimum pedal force values indicated the forces were directed opposite to the rotation of the crank arm and pedal spindle.

Table 3: Average Pedal Force Component Tangent to Crank Arm Path

Subject	Maximum Force (SD) Newtons	Minimum Force (SD) Newtons
0	186 (5)	-64 (4)
1	167 (22)	-96 (13)
3	162 (15)	-59 (6)
4	143 (11)	-93 (13)
6	167 (14)	-77 (7)
7	186 (20)	-89 (9)
8	148 (18)	-77 (6)
9	168 (16)	-94 (7)
10	188 (18)	-89 (5)
11	212 (8)	-103 (4)
Grand Mean	173 (24)	-84 (16)

Presented in Table 4 below, the timing angle of the maximum force component tangent to the crank arm path ranged from 81° (4°) to 119° (8°), with a grand mean of 104° (13°). The timing angle of the minimum tangent force ranged from 271° (33°) to 289° (8°), with a grand mean of 281° (14°) across all subjects.

Table 4: Angle at which the Applied Maximum and Minimum Force Component
Tangent to the Left Crank Arm Path Occurred (Timing Angle)

Subject	Maximum Force Angle Degrees (SD)	Minimum Force Angle Degrees (SD)
0	103 (8)	287 (10)
1	97 (8)	289 (8)
3	105 (14)	283 (6)
4	100 (9)	287 (11)
6	109 (7)	285 (8)
7	81 (4)	271 (33)
8	119 (8)	288 (5)
9	107 (3)	271 (4)
10	117 (5)	281 (6)
11	105 (5)	273 (13)
Grand Mean	104 (13)	281 (14)

The lateral, or side to side pedal forces were measured at both the right and left pedal. This force component was independent of the pedal surface angle in the plane of the cycle, unlike the pedal force component tangent to the crank arm path mentioned above. It should first be noted that in the laboratory coordinate system, a positive force value is directed away from the cycle as measured at the right pedal, as is a negative force value at the left pedal. The magnitude of the right pedal lateral force (Table 5) ranged from 33N (10N) to 52N (2N) with a grand mean of 41N (7N) at the right pedal, and -26N (3) to -54N (2) with a grand mean of -38N (10) at the left pedal.

Table 5: Lateral (side to side) Right and Left Pedal Maximum Forces; Forces directed away from cycle were positive on the right and negative on the left

Subject	Right Pedal Maximum Force (SD) Newtons	Left Pedal Maximum Force (SD) Newtons
0	48 (2)	-54 (2)
1	33 (10)	-34 (12)
3	38 (3)	-50 (5)
4	36 (3)	-26 (3)
6	37 (3)	-30 (3)
7	42 (6)	-41 (7)
8	38 (3)	-30 (6)
9	43 (6)	-39 (3)
10	45 (5)	-40 (5)
11	52 (2)	-39 (1)
Grand Mean	41 (7)	-38 (10)

The timing angle associated with the right maximum lateral pedal forces (Table 6) ranged from 278° (16°) to 334° (20°), with a grand mean of 299° (17°). The timing angle associated with the maximum lateral left pedal force ranged from 96° (33°) to 131° (4°), with a grand mean of 116° (16°).

Table 6: Timing Angle of Maximum Lateral Pedal Force

Subject	Right Timing Angle Degrees (SD)	Left Timing Angle Degrees (SD)
0	288 (5)	104 (6)
1	334 (20)	96 (33)
3	293 (7)	121 (13)
4	303 (5)	116 (8)
6	278 (16)	117 (5)
7	302 (8)	105 (8)
8	305 (7)	119 (11)
9	288 (4)	120 (4)
10	297 (5)	128 (10)
11	303 (5)	131 (4)
Grand Mean	299 (17)	116 (16)

The minimum lateral forces at the pedals were directed towards the cycle, as indicated by the negative value (Table 7) on the right pedal and the positive value on the left pedal. The minimum lateral force measured at the surface of the right pedal ranged from 0N (1N) to -10N (5N), with a grand mean of -5N (4N) across all subjects. The minimum lateral force measured at the surface of the left pedal ranged from 0N (1N) to 16N (2N), with a grand mean of 7N (4N).

Table 7: Minimum Right and Left Pedal Lateral Forces;
Forces directed towards the cycle were
negative on the right pedal and positive on the left

Subject	Right Pedal Minimum Force (SD) Newtons	Left Pedal Minimum Force (SD) Newtons
0	-5 (1)	0 (1)
1	-2 (6)	6 (3)
3	-3 (1)	8 (3)
4	-5 (3)	8 (2)
6	-10 (5)	5 (2)
7	0 (1)	3 (2)
8	-6 (3)	10 (3)
9	-6 (1)	7 (1)
10	-8 (4)	16 (2)
11	-5 (1)	9 (1)
Grand Mean	-5 (4)	7 (4)

The timing angles of the minimum lateral pedal forces were approximately 113° (38°) for the right pedal and 275° (48°) for the left pedal. There was more variability, as represented by the larger standard deviations, in the timing angle of the minimum lateral pedal forces than the maximum lateral pedal forces.

Table 8: Timing Angle of Minimum Lateral Pedal Forces

Subject	Right Timing Angle Degrees (SD)	Left Timing Angle Degrees (SD)
0	117 (32)	254 (47)
1	125 (44)	326 (25)
3	127 (18)	241 (17)
4	94 (27)	272 (41)
6	98 (49)	280 (97)
7	89 (13)	279 (5)
8	103 (20)	232 (24)
9	105 (11)	311 (8)
10	114 (58)	245 (4)
11	156 (36)	313 (4)
Grand Mean	113 (38)	275 (48)

The range between the minimum and maximum lateral force of the right lateral pedal forces varied from 36N (14N) to 56N (4N) with a grand mean of 46N (9N) across all subjects. For the left pedal, the range varied from 35N (4N) to 58N (6N) with a grand mean of 45N (10N).

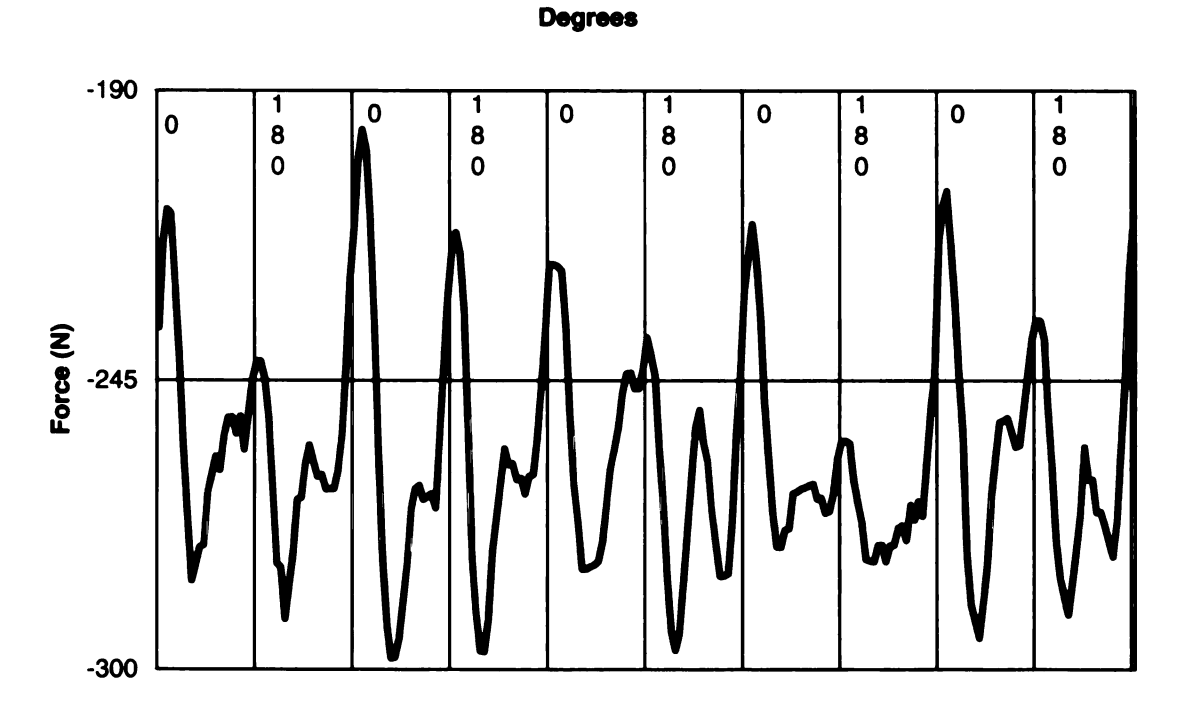
Table 9: Range between Maximum and Minimum Lateral Pedal Forces

Subject	Right Pedal Newtons (SD)	Left Pedal Newtons (SD)
0	53 (2)	54 (3)
1	36 (14)	41 (13)
3	41 (3)	58 (6)
4	41 (4)	34 (4)
6	47 (5)	35 (4)
7	42 (6)	43 (8)
8	44 (4)	40 (6)
9	49 (5)	46 (3)
10	53 (7)	55 (6)
11	56 (4)	48 (2)
Grand Mean	46 (9)	45 (10)

Seat Vertical Forces

Shown in Figure 16 is representative data of the vertical seat force over five crank arm revolutions gathered from a single trial of one subject. The vertical force at the seat

Figure 16: Vertical Seat Force Profile over Five Crank Arm Revolutions; Single subject



exhibited a "double cycle" force profile per revolution of the crank arm.

The magnitude of the maximum vertical seat forces for all ten subjects ranged from 285N (7N) to 472N (12N), with a grand mean of 372N (56N) during 0-180° and 369N (48N) during 180-360° of the crank arm revolution. In terms of percentage body weight, while the left leg was driving the maximum vertical load on the seat averaged across the subjects was 52% (6%) of the subject's body weight (% BW), and 51% (5%) BW while the right leg was driving. The maximum vertical seat force always acted downward on the cycle, or upward on the rider's groin. The maximum vertical seat force values for all subjects are shown in Table 10.

Table 10: Maximum Seat Vertical Force and Standard Deviation (SD) for the Regular Position;

Negative values indicate a force directed towards the ground

Subject	0-180° Force(SD) Newtons	Percent Body Weight	180-360° Force(SD) Newtons	Percent Body Weight
0	-285 (7)	45% (1%)	-291 (6)	46% (1%)
1	-393 (9)	56% (1%)	-343 (18)	49% (3%)
3	-310 (10)	44% (1%)	-325 (8)	47% (1%)
4	-472 (12)	61% (2%)	-456 (7)	59% (1%)
6	-362 (13)	52% (2%)	-350 (13)	50% (2%)
7	-396(19)	55% (3%)	-381 (16)	53% (2%)
8	-438 (22)	58 (3%)	-413 (7)	55% (1%)
9	-326 (7)	47% (1%)	-333 (11)	48% (2%)
10	-361 (14)	54% (2%)	-371 (12)	55% (2%)
11	-374 (10)	47% (1%)	-373 (6)	47% (1%)
Grand Mean	-372 (56)	52% (6%)	-364 (46)	51% (4%)

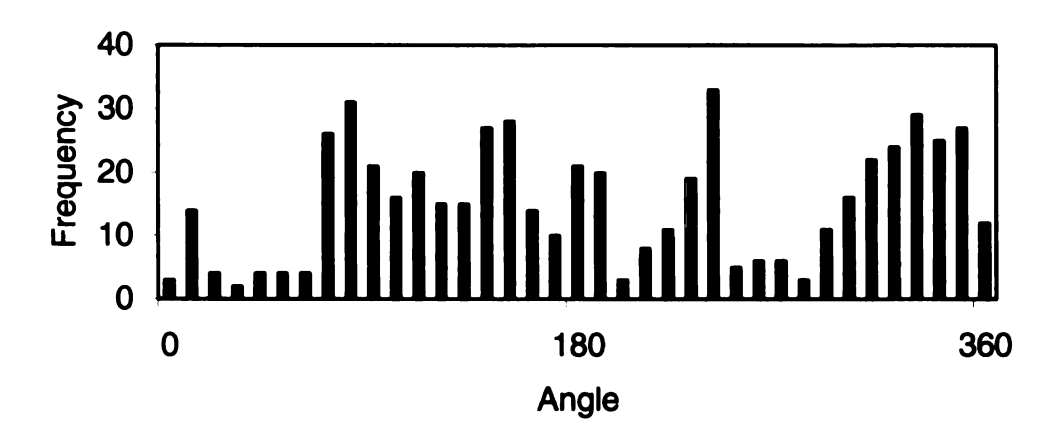
Table 11: Timing Angles at which the Maximum Vertical Seat Forces Occurred

	0-180°	180-360°
Subject	Angle ^o (SD)	Angle ^o (SD)
0	72 (8)	234 (4)
1	157 (12)	292 (33)
3	85 (30)	301 (12)
4	109 (6)	280 (28)
6	120 (19)	315 (30)
7	132 (5)	317 (6)
8	173 (7)	343 (5)
9	77 (34)	324 (30)
10	80 (22)	216 (9)
11	81 (11)	262 (41)
Grand Mean	108 (38)	288 (45)

Due to the variation seen in the timing angles for the maximum seat vertical force (SD where about 20-25% of their respective regions of the crank arm revolution), another

method was attempted to describe this timing angle. However, a plot that described the number of occurrences for the timing angle at the maximum vertical seat force, Figure 17, also showed no clear region in the crank arm revolution where the maximum vertical seat forces occurred.

Figure 17: Maximum Vertical Seat Force Timing Angle Histogram



The magnitude of the minimum vertical seat forces ranged from 202N (12N) to 382N (11N), and again acted in the downward direction on the cycle. Across all subjects, the grand mean was 292N (49N) for 0-180° and 291N (44N) for 180-360°. After normalized with respect to body weight, the grand mean of the minimum vertical seat forces of all the subjects was 41% (6%) BW during 0-180° and 41% (5%) BW during 180-360° of the crank arm revolution.

Table 12: Minimum Seat Vertical Force and Standard Deviation (SD) for the Regular position;
Negative values indicated a force directed downward

Subject	0-180° Force(SD) Newtons	Percent Body Weight	180-360° Force(SD) Newtons	Percent Body Weight
0	-202 (12)	32% (2%)	-222 (13)	35% (2%)
1	-293 (10)	42% (2%)	-298 (17)	43% (3%)
3	-251 (15)	36% (2%)	-253 (19)	36% (3%)
4	-377 (12)	48% (2%)	-382 (11)	49% (1%)
6	-319 (17)	46% (2%)	-302 (7)	44% (1%)
7	-275 (17)	38% (2%)	-276 (10)	38% (1%)
8	-350 (16)	47% (2%)	-335 (21)	44% (3%)
9	-283 (12)	40% (2%)	-278 (10)	40% (1%)
10	-286 (15)	43% (2%)	-290 (8)	43% (1%)
11	-279 (11)	35% (1%)	-279 (11)	35% (1%)
Grand Mean	-292 (49)	41% (6%)	-291 (44)	41% (5%)

The timing angles of the minimum seat vertical forces were 73° (75°) while the left leg was driving and 243° (82°) while the right leg was driving. As can be seen in Table 13, the standard deviations of the timing angle were greater than half of the range they were measured over in some subjects, for example 111° in Subject 7.

Table 13: Timing Angle of Minimum Seat Vertical Forces

Subject	0-180° Angle (SD)°	180-360° Angle (SD)
0	13 (6)	254 (87)
1	78 (42)	288 (55)
3	139 (64)	186 (3)
4	63 (78)	239 (82)
6	30 (29)	255 (59)
7	43 (111)	321 (73)
8	34 (4)	223 (3)
9	53 (64)	201 (28)
10	111 (73)	288 (117)
11	161 (54)	169 (100)
Grand Mean	73 (75)	243 (82)

Similar to the timing angles of the maximum vertical seat forces, the grand mean timing angles for the minimum vertical seat forces were difficult to interpret, with the standard deviations of 75° and 82° during 0-180° and 180-360°, respectively. Another method of analysis provided a more informative description of the timing angles. This was done with a histogram, Figure 18, which described the frequency of occurrence for the timing angles at the minimum vertical seat forces. It was observed that the minimum vertical seat forces occurred at a much higher frequencies over the ranges of 170°-230°

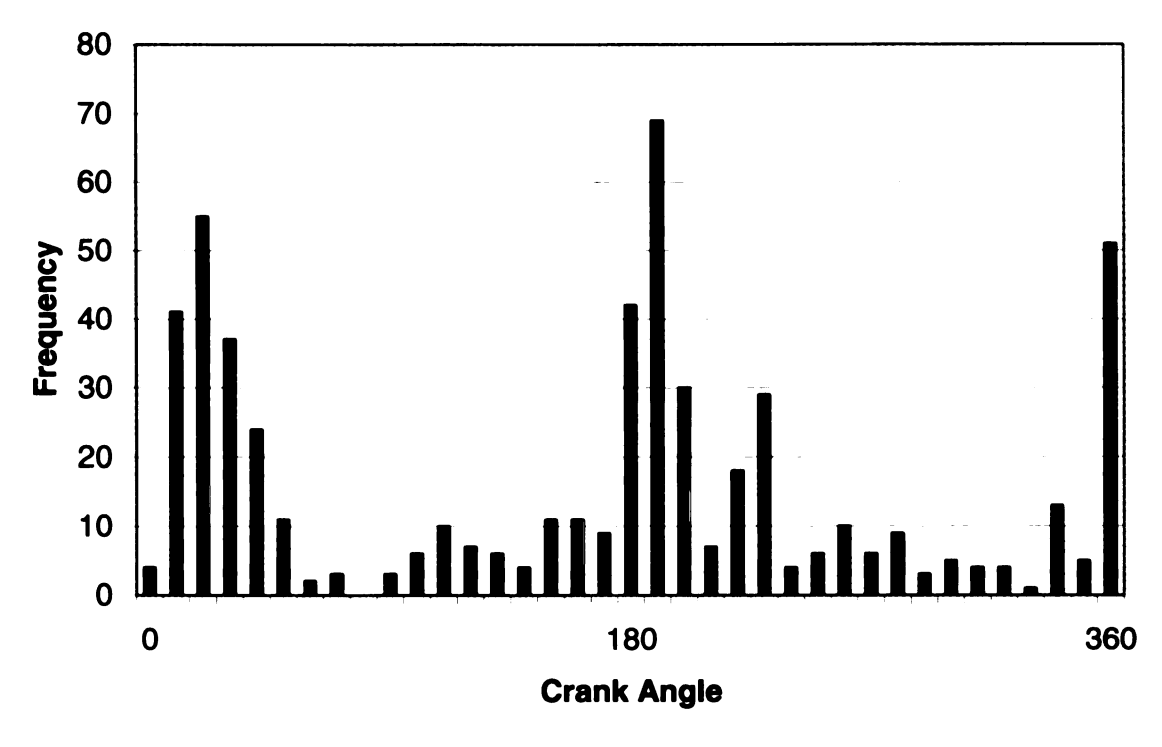


Figure 18: Minimum Seat Vertical Force Timing Angle Frequency

(35% of values) and also from 350°-40° (38% of the values). Together these regions contained a total of 73% of the timing angles at the minimum seat vertical force.

The range between the maximum and minimum vertical seat forces was then calculated to reveal the difference in magnitude between them. The range of the vertical seat force varied from 43N (12N) to 121N (14N) during 0-180° and 45N (17N) to 105N

(12N) during 180-360°. Across all subjects the grand mean difference between the maximum and minimum mean seat vertical force was 80N (28N) for 0-180° and 72N (24N) for 180-360°. In terms of percent body weight, the differences in the vertical seat forces were approximately 11% (4%) for 0-180° and 10% (3%) for 180-360°. It should again be noted that the vertical seat forces were always directed downward on the cycle.

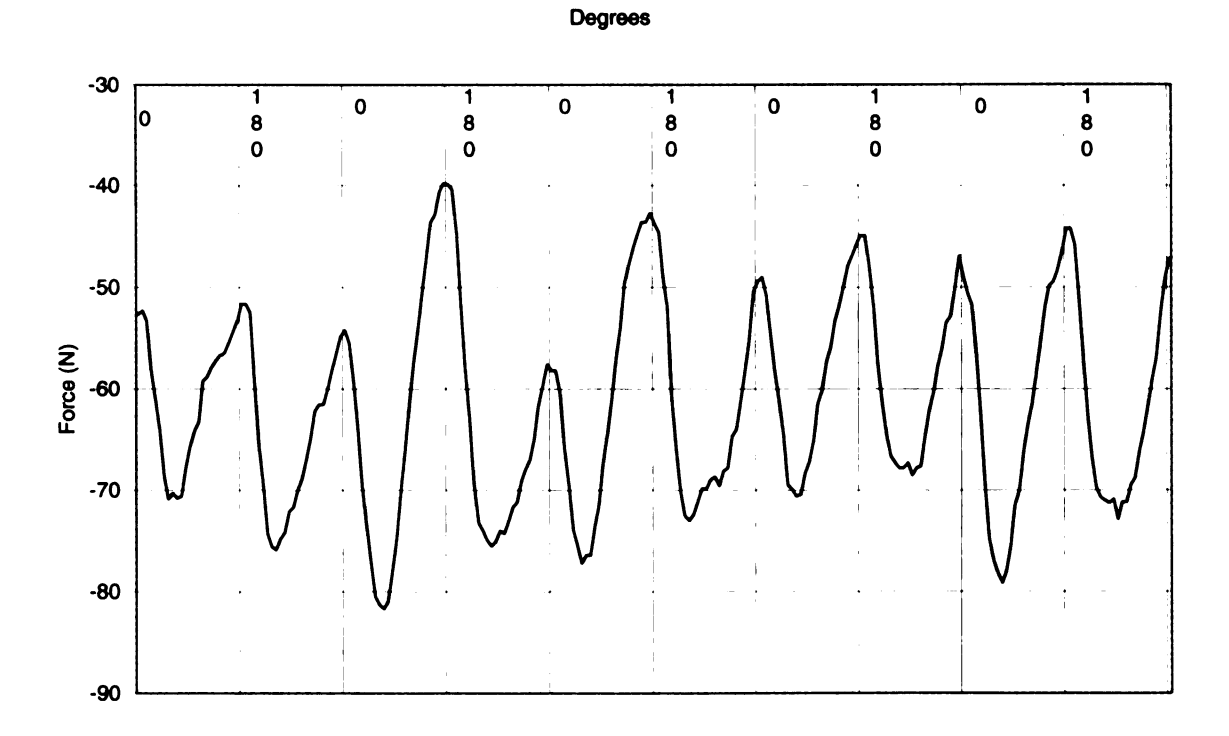
Table 14: Range between the Maximum and Minimum Vertical Seat Forces

Subject	0-180° Vertical Force Range Newtons (SD)	Percent Body Weight (SD)	180-360° Vertical Force Range Newtons (SD)	Percent Body Weight (SD)
0	83 (16)	13% (3%)	69 (17)	11% (3%)
1	99 (13)	14% (2%)	45 (17)	6 (2%)
3	58 (20)	8% (3%)	72 (23)	10 (3%)
4	95 (7)	12% (1%)	74 (8)	10 (0%)
6	43 (16)	6% (2%)	47 (16)	7 (2%)
7	121 (14)	17% (2%)	105 (12)	15 (2%)
8	87 (21)	12% (3%)	78 (23)	10 (3%)
9	43 (12)	6% (2%)	55 (16)	8 (2%)
10	75 (13)	11% (2%)	80 (11)	12 (2%)
11	95 (18)	12% (2%)	94 (11)	12 (1%)
Grand				
Mean	80 (28)	11% (4%)	72 (24)	10% (3%)

Forward/Rearward Seat Forces

A representative forward/rearward (FR), seat force profile for five full crank arm revolutions of a single subject is shown in Figure 19.

Figure 19: Forward/Rearward (FR) Seat Force Profile over Five Subsequent Crank
Arm Revolutions; Single trial for one subject



Across all 10 subjects, the maximum magnitude of the FR seat force in the Regular position ranged from 41N (12N) to 111N (6N), with a grand mean of 78N (20N) that occurred while the left leg was driving (0-180°) and 79N (22N) while the right leg was driving (180-360°). The maximum FR force as a percentage of body weight across all subjects was 11% (3%) while the left leg was driving and 11% (3%) while the right leg was driving. As indicated by the negative values presented in Table 15, the maximum magnitude of the FR seat force was always directed in the rearward direction on the cycle.

Table 15: Maximum Forward/Rearward (FR) Seat Force Negative Values Indicate a Force Directed Towards the Rear of the Cycle

Subject	0-180° Force(SD) Newtons	Percent Body Weight	180-360° Force(SD) Newtons	Percent Body Weight
0	-75 (5)	12% (1%)	-75 (3)	12% (1%)
1	-55 (11)	8% (2%)	-47 (19)	7% (3%)
3	-70 (6)	10 (1%)	-81 (8)	12% (1%)
4	-84 (9)	11% (1%)	-81 (5)	10% (1%)
6	-41 (12)	5% (2%)	-45 (11)	7% (2%)
7	-96 (3)	13% (0%)	-93 (5)	13% (1%)
8	-88 (9)	11% (1%)	-82 (8)	11% (1%)
9	-102 (5)	15% (1%)	-111 (6)	16% (1%)
10	-72 (9)	11% (1%)	-65 (15)	10% (1%)
11	-96 (5)	12% (1%)	-107 (5)	13% (1%)
Grand Mean	-78 (20)	11% (3%)	-79 (22)	11% (3%)

The timing angle of the maximum FR shear force occurred across all subjects at approximately 81° (22°) while the left leg was driving and 267° (25°) while the right leg was driving. Some of the variability may have been due to the frequency at which motion data was sampled (60Hz). With the subject's maintaining a crank arm frequency of 75 RPM, one frames difference was approximately equal to 7.5° of crank arm rotation. The phase difference between the driving regions was slightly greater than 180° albeit with similar variability, and the difference may be explained by a subject that favored a dominant leg (Smak et al. 1999), or some other musculoskeletal asymmetry in the subject.

Table 16: Maximum Forward/Rearward Seat Force Timing Angles

	0-180°	180-360°
Subject	Angle(SD)°	Angle(SD)
0	69 (11)	260 (14)
1	88 (17)	286 (13)
3	68 (19)	249 (9)
4	106 (11)	293 (10)
6	87 (29)	274 (17)
7	73 (8)	270 (6)
8	94 (23)	256 (20)
9	69 (30)	277 (46)
10	65 (14)	259 (31)
11	90 (5)	251 (6)
Grand Mean	81 (22)	268 (25)

The minimum FR seat shear, Table 17, ranged from 0N (11N) to 85N (4N) with a grand mean of 39N (22N) during 0-180° of a crank arm revolution, and 39N (22N) during 180-360°. In terms of percent body weight (%BW), the minimum mean FR seat shear is approximately 5% BW (3%) during 0-180° and 6% BW (3%) during 180-360°. Similar

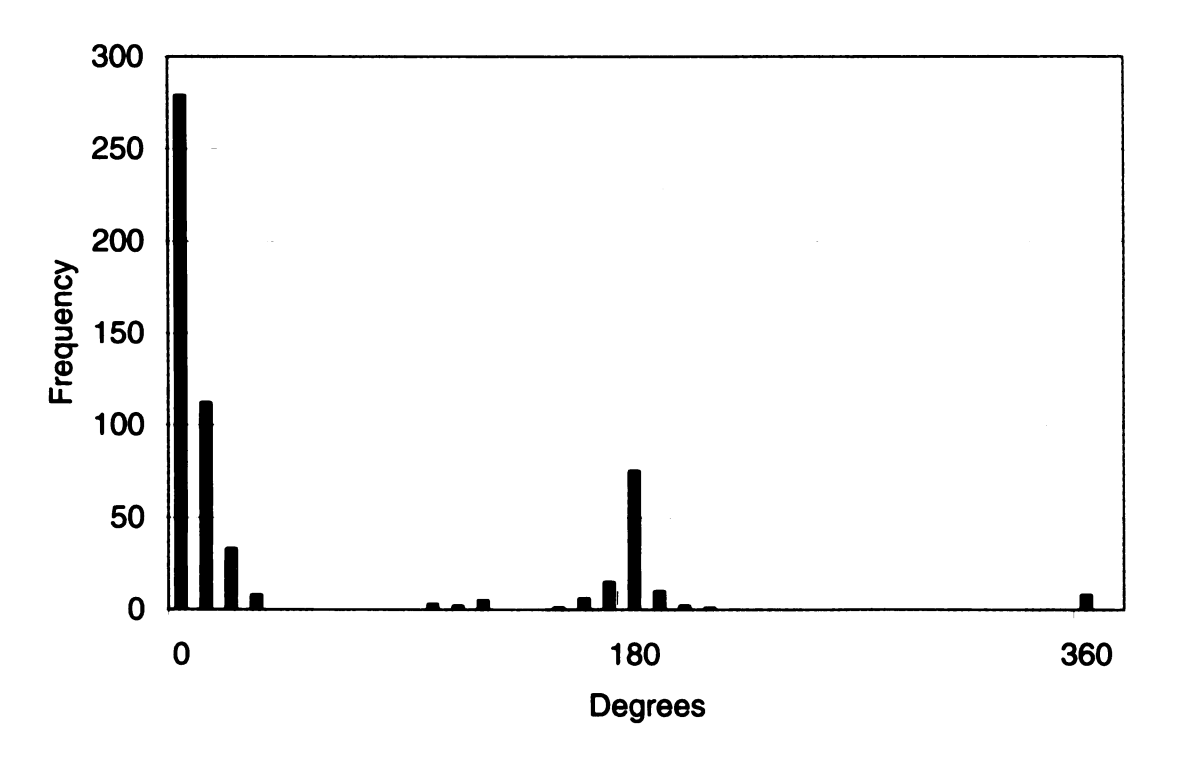
to the maximum mean FR seat shear, the minimum mean FR seat shear was always directed in the rearward direction as indicated by the negative sign for the force values.

Table 17: Minimum FR Seat Shear Forces; Negative values indicated that the forces were directed towards the rear of the cycle

Subject	0-180° Force(SD) Newtons	Percent Body Weight	180-360° Force(SD) Newtons	Percent Body Weight
0	-43 (5)	7% (1%)	-42 (4)	7% (1%)
1	-6 (13)	1% (1%)	-0 (11)	0% (2%)
3	-47 (4)	7% (1%)	-46 (4)	7% (1%)
4	-40 (5)	5% (1%)	-45 (5)	6% (1%)
6	-13 (12)	2% (2%)	-12 (12)	2% (2%)
7	-39 (1)	5% (0%)	-39 (5)	5% (1%)
8	-35 (10)	5% (1%)	-38 (8)	5% (1%)
9	-85 (4)	12% (1%)	-83 (4)	12% (1%)
10	-36 (8)	5% (1%)	-37 (8)	6% (1%)
11	-50 (3)	6% (0%)	-52 (7)	6% (1%)
Grand Mean	-39 (22)	5% (3%)	-39 (22)	6% (3%)

The FR shear forces at the seat generally reached their minimum magnitudes and inflected in the region when either leg was at its maximum height during a crank arm revolution, i.e. 0° and 180° . Although this was readily apparent for the force profile of the subject shown previously in Figure 19, it was difficult to confirm a mean using normal data reduction techniques when the timing angle values occurred at inconsistent angles such as $0^{\circ} = 360^{\circ}$. To better illustrate the timing angle for the minimum FR seat force magnitude, a histogram of the frequency of timing angle values was plotted in Figure 20. With only a few exceptions, the minimum FR seat forces were clustered in the regions near 0° and 180° , with 76% of the values in the range of $0-20^{\circ}$ and 18% between $160-190^{\circ}$.





The range between the maximum and minimum FR seat force varied from 16N (6N) for subject 9 to 57N (3N) for subject 7, with a grand mean of 39N (15N) while the left leg was driving, and from 27N (8N) to 55N (7N) with a grand mean of 39N (13N) while the right leg was driving.

Table 18: Range between the Maximum and Minimum FR Seat Forces

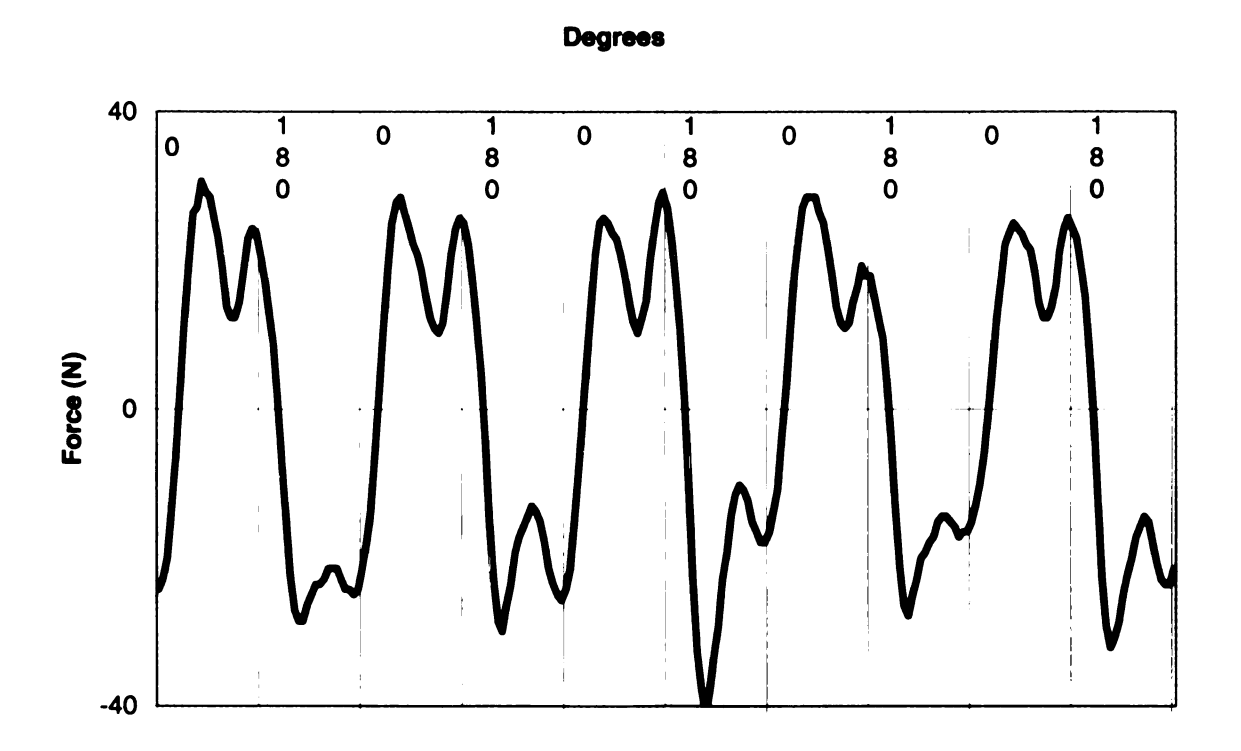
Subject	0-180° Range (SD) Newtons	180-360° Range (SD) Newtons
0	32 (7)	33 (6)
1	48 (11)	47 (17)
3	23 (8)	35 (9)
4	45 (12)	36 (8)
6	28 (8)	33 (8)
7	57 (3)	53 (8)
8	54 (6)	44 (9)
9	16 (6)	27 (8)
10	36 (13)	28 (7)
11	46 (5)	55 (7)
Grand Mean	39 (15)	39 (13)

Lateral Seat Forces

The lateral (side to side) seat force profiles displayed a single cycle of data per crank arm revolution. Although this seems not to be similar with the vertical and FR seat forces (which exhibited two force cycles per crank arm revolution), this force was the only one that changed direction from right lateral during approximately 0-180° (a positive force value), decreased to zero, then increased directed left laterally during 180-360° (a negative force value). This change in direction showed as a sign difference in the force magnitude measured by the load cell.

Two distinct profiles of the lateral seat forces became apparent within the group of subjects tested. Although both profiles exhibit a single cycle of force data for every complete revolution of the crank arms, one pattern was characterized by a "double hump", Figure 21 below. Three inflection points occurred during each phase (i.e. 0-180° and 180-360°) of the crank arm revolution, and was seen in six of the ten subjects (0, 1, 3, 6, 7, and 9).

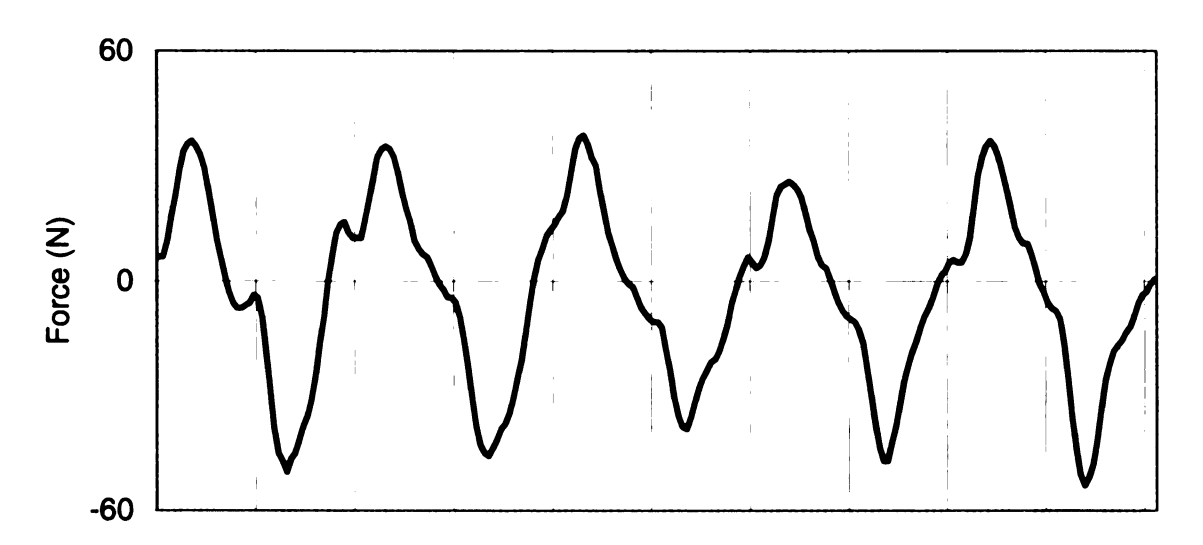
Figure 21: "Double Hump" Lateral Seat Force Profile; Single subject, single test



The remaining subjects (4, 8, 10, and 11) showed a "single hump" force profile per portion of the crank arm cycle, shown in Figure 22. As the left leg was driving the

Figure 22: "Single Hump" Lateral Seat Force Profile; Subject 4, Test 5

Degrees



crank arms the lateral seat force was directed away from the cycle to the right and similarly, while the right leg was driving the lateral seat force was directed to the left of the cycle.

With the left leg driving, the maximum lateral seat forces ranged from 20N (5N) for subject 8 to 44N (7N) for subject 1 and were directed right laterally. The grand mean was 31N (8N) and corresponded to a mean value of 4% BW (1%) across all subjects. While the right leg was driving the lateral force magnitudes ranged from 22N (3N) to 46N (6N) and were directed left laterally, with a grand mean of 33N (8N). These forces were equivalent to 5% BW (1%) across all subjects.

Table 19: Maximum Lateral Seat Forces;
Positive values were directed right lateral, negative values left lateral
(*-indicates subject displayed "Double Hump" Force Profile)

Subject	0-180° Force (SD) Newtons	Percent Body Weight	180-360° Force (SD) Newtons	Percent Body Weight
0*	31 (4)	5% (1%)	-29 (5)	5% (1%)
1*	44 (7)	6% (1%)	-26 (5)	4% (1%)
3*	29 (4)	4% (1%)	-28 (4)	4% (1%)
4	34 (4)	4% (1%)	-46 (6)	6% (1%)
6*	24 (8)	3% (1%)	-22 (3)	3% (0%)
7*	34 (9)	5% (1%)	-34 (9)	5% (1%)
8	20 (5)	3% (1%)	-35 (7)	5% (1%)
9*	35 (4)	5% (1%)	-36 (3)	5% (0%)
10	26 (7)	4% (1%)	-36 (8)	5% (1%)
11	30 (3)	4% (0%)	-37 (6)	5% (1%)
Grand Mean	31 (8)	4% (1%)	-33 (8)	5% (1%)

The timing angles of the maximum lateral seat forces ranged from 62° (4°) for subject 7 to 155° (16°) for subject 9, with a grand mean of 92 (43) while the left leg was driving. While the right leg was driving, the timing angles ranged from 240 (10) to 329 (30), with a grand mean of 266 (42). Standard deviations of approximately one third of the evaluated regions occurred in several of the subjects, and were also reflected in the standard deviations of the grand means. As examples, subject 3 showed a SD of 54° while the left leg was driving (0-180°), while subject 1 showed an SD of 58° while the right leg was driving.

Table 20: Lateral Seat Force Timing Angles (*-indicates "Double Hump" Force Profile)

Subject	0-180° Angle(SD)°	180-360° Angle(SD)
0*	99 (49)	256 (31)
1*	113 (43)	290 (58)
3*	108 (54)	251 (36)
4	62 (4)	240 (5)
6*	93 (53)	329 (30)
7*	63 (4)	240 (10)
8	92 (37)	243 (32)
9*	155 (16)	309 (44)
10	72 (9)	252 (17)
11	63 (4)	252 (7)
Grand Mean	92 (43)	266 (42)

The range between the maximum lateral seat force magnitudes varied from 46N (9N) in subject 6 to 79N (8N) in subject 4, with a grand mean of 63N (12N) across all of the subjects.

Table 21: Range of Maximum Lateral Seat Forces

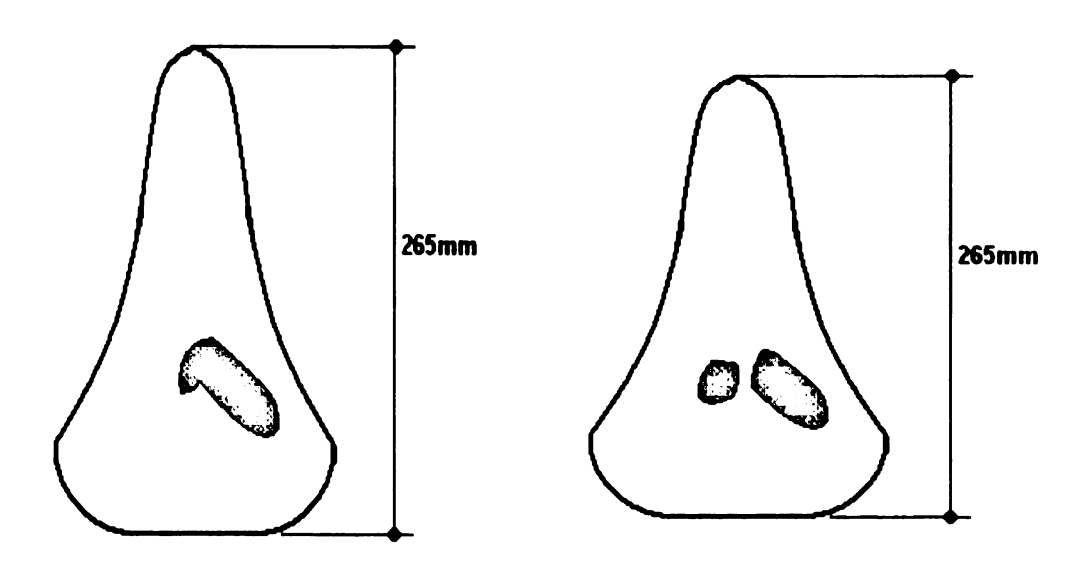
Subject	Force (SD)
	Newtons
0	60 (5)
1	69 (8)
3	57 (6)
4	79 (8)
6	46 (9)
7	68 (15)
8	55 (9)
9	71 (5)
10	62 (11)
11	67 (7)
Grand Mean	63 (12)

Seat Pressure Mapping

Mapped pressure data from the seat were qualitatively analyzed to estimate regions of contact that occurred between the seat and the subject's pelvis and groin. The pressure zones showing the greatest contact appeared to repetitively map out the shape of the mid to anterior region subject's pelvis over time. However, not immediately intuitive were the patterns of moving contact regions between the seat and rider, especially at the timing angles of the maximum seat forces.

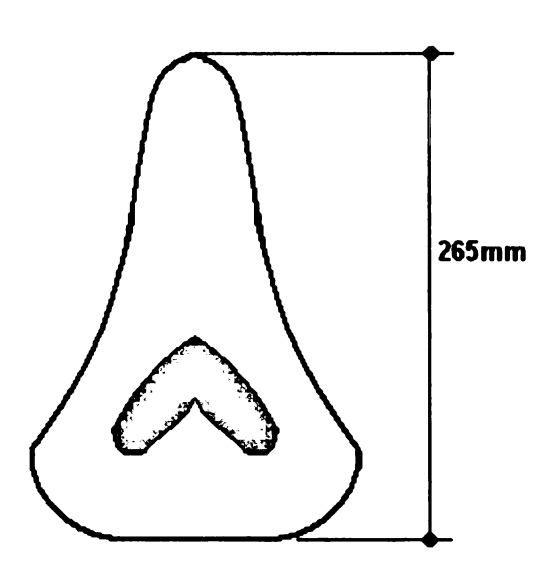
In the regions of the crank arm revolution when the maximum vertical seat force occurred, pressure data indicated greater contact on the opposite side of the seat from the driving leg, and two similar patterns were noticed amongst the subjects tested. For example, in the case where the left leg was driving the crank arms, mapped pressure showed increased contact along the right side of the seat, as seen in Figure 23 below.

Figure 23: Top View of Seat Pressure Maps; Regions of greatest contact (pressure > 3.1 N/cm²) at the maximum vertical seat force while the left leg was driving



The maximum FR and lateral shearing seat forces occurred at approximately the same timing angles during a crank arm revolution. These timing angle regions (approximately 90° and 270°) presented the most anterior (furthest forward) regions of contact between the rider and seat in the pressure data during a revolution of the crank arms. The largest pressure magnitudes measured were greater than 3.10 N/cm² (4.5 psi) and appeared concentrated along the anterior pelvic ridge (bilaterally, the pubic ramii) independent of the driving leg. When the maximum FR and lateral seat forces occurred,

Figure 24: Seat Pressure Map; Timing of the maximum FR and lateral seat forces. Grey regions indicated the greatest contact areas between the seat and rider (>3.1 N/cm²)



it appeared that the subject's pelvis was rotated forward such that the rear regions of the pelvis (the ischial tuberosities, or ITs) and buttocks supported no body weight.

Interestingly, this section of the seat was not contoured in the forward/rearward or lateral directions, which indicated that the measured FR and lateral seat forces were likely

actual shear forces, rather than applied forces normal to the seat surface with some forward/rearward contour orientation.

Handlebar Vertical Forces

In the Regular handlebar position, the maximum vertical handlebar forces ranged from 55N (7N) to 107N (5N), and had a grand mean of 80N (15N) for the right handlebar and 79N (15N) for the left handlebar. When normalized with respect to body weight it was found that a maximum force equivalent to 11% (2%) of the body acted on each handlebar that was always directed on the cycle towards the ground.

Table 22: Maximum Handlebar Vertical Force; Negative values indicated a force directed downward

Subject	Right Vertical Force (SD) Newtons	Percent Body Weight (SD)	Left Vertical Force (SD) Newtons	Percent Body Weight (SD)
0	-80 (3)	13% (0%)	-64 (2)	10% (0%)
1	-55 (7)	8 (1%)	-75 (11)	11% (2%)
3	-81 (4)	12% (1%)	-99 (4)	14% (1%)
4	-72 (3)	9% (0%)	-73 (2)	9% (0%)
6	-69 (11)	10% (2%)	-55 (6)	8% (1%)
7	-91 (3)	13% (0%)	-79 (5)	11% (1%)
8	-107 (5)	14% (1%)	-89 (4)	12% (1%)
9	-81 (4)	12% (1%)	-82 (4.4)	12% (1%)
10	-70 (4)	10% (1%)	-67 (5)	10% (1%)
11	-95 (3)	12% (0%)	-102 (2)	13% (0%)
Grand Mean	-80 (15)	11% (2%)	-79 (15)	11% (2%)

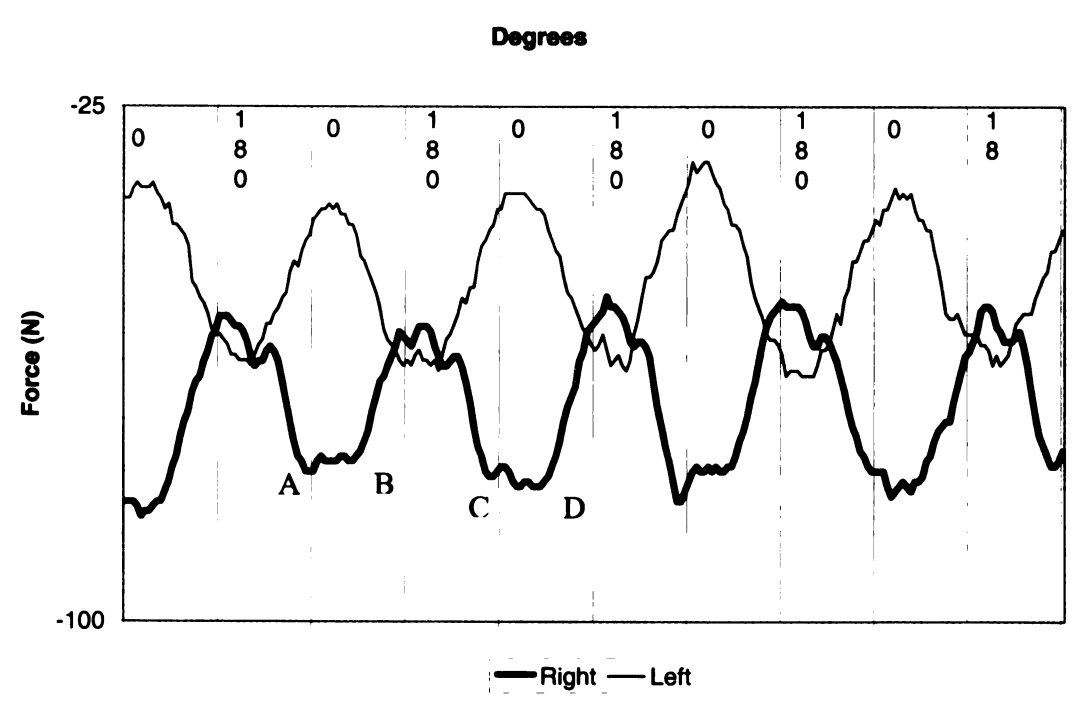
The timing angle of the maximum handlebar forces varied across the subjects, with a range of 7° (22°) to 74° (9°) for the right handlebar and 183° (26°) to 236° (5°) for the left handlebar. The grand mean across the subjects was 44° (44°) for the right handlebar and 217° (37°) for the left handlebar.

Table 23: Timing Angle of the Maximum Vertical Handlebar Force

Subject	Right Handlebar Angle (SD)	Left Handlebar Angle (SD)
0	7 (22)	221 (24)
1	54 (43)	245 (60)
3	45 (24)	234 (20)
4	61 (70)	228 (34)
6	54 (38)	226 (17)
7	16 (38)	183 (26)
8	72 (28)	187 (10)
9	34 (45)	229 (31)
10	29 (52)	219 (32)
11	74 (9)	236 (5)
Grand Mean	44 (44)	221 (34)

When the profiles of the right and left handlebar forces were viewed, it was apparent that their standard deviations, presented in Table 23 above, may have resulted from the somewhat flat regions of force data that contained the maximum magnitude in some of the cycles. These regions were represented from points A-B and C-D in the handlebar vertical force profile shown in Figure 25 below. It was clear that the maximum magnitude at point A occurred in the beginning of the region, while for a subsequent

Figure 25: Handlebar Vertical Force Profile; Single subject in the Regular position



cycle the maximum magnitude occurred at point D.

The minimum vertical force on the right handlebar ranged from -29N (8N) to -72N (3N) with a grand mean of -52N (13N). The minimum vertical force on the left handlebar ranged from -35N (3N) to -73N (3N) with a grand mean of -48N (11N). Again, the negative force values indicated a direction towards the ground on the cycle.

These forces ranged from the equivalent of 4% (1%) to 9% (0%) BW with a grand mean of 7% (2%) BW on the right handlebar, and 5% (0%) to 9% (0%) BW with a grand mean of 7% (1%) BW on the left handlebar.

Table 24: Minimum Handlebar Vertical Force Negative Values Indicated a Force Directed Towards the Ground

Subject	Right Vertical Force (SD) Newtons	Percent Body Weight (SD)	Left Vertical Force (SD) Newtons	Percent Body Weight (SD)
0	-52 (3)	8% (1%)	-35 (3)	6% (1%)
1	-29 (8)	4% (1%)	-46 (9)	7% (1%)
3	-45 (4)	6% (1%)	-49 (5)	7% (1%)
4	-50 (4)	6% (0%)	-52 (2)	7% (0%)
6	-45 (6)	7% (1%)	-36 (3)	5% (0%)
7	-59 (7)	8% (1%)	-43 (7)	6% (1%)
8	-68 (5)	9% (1%)	-46 (5)	6% (1%)
9	-57 (4)	8% (1%)	-56 (3)	8% (0%)
10	-45 (4)	7% (1%)	-45 (2)	7% (0%)
11	-72 (3)	9% (0%)	-73 (3)	9% (0%)
Grand Mean	-52 (13)	7% (2%)	-48 (11)	7% (1%)

The timing angles for the minimum magnitude of vertical forces at the handlebars ranged from 192° (20°) to 279° (7°) on the right handlebar and 17° (13°) to 54° (41°) for the left handlebar. The grand mean timing angle was 229° (28°) on the right handlebar and 33° (30°) on the left handlebar. The standard deviations of 28° (right) and 30° (left) in the grand mean timing angles represented approximately 8% of a full crank arm revolution.

Table 25: Timing Angle of the Minimum Vertical Handlebar Load

Subject	Right Handlebar Angle° (SD)	Left Handlebar Angle ^o (SD)
0	192 (20)	31 (18)
1	232 (25)	35 (60)
3	227 (20)	49 (21)
4	239 (15)	38 (19)
6	235 (28)	26 (22)
7	216 (15)	19 (16)
8	232 (21)	17 (13)
9	223 (8)	32 (19)
10	217 (20)	28 (33)
11	279 (7)	54 (41)
Grand Mean	229 (28)	33 (30)

The range between the maximum and minimum vertical handlebar forces varied from 22N (6N) to 39N (4N), or 4% (1%) to 5% (1%) BW, and had a grand mean of 28N (7N) (4% (1%)BW) on the right handlebar. On the left handlebar, the range varied from 19N (5N) to 50N (6N), or 3% (1%) to 7% (1%) BW, and had a grand mean of 30N (11N) or 4% (1%) BW. Again, the maximum and minimum vertical handlebar forces were always directed toward the ground on the cycle.

Table 26: Range between the Maximum and Minimum Vertical Handlebar Forces

Subject	Right Vertical Force (SD) Newtons	Percent Body Weight (SD)	Left Vertical Force (SD) Newtons	Percent Body Weight (SD)
0	28 (3)	4% (0%)	28 (3)	4% (0%)
1	26 (6)	4% (1%)	30 (7)	4% (1%)
3	36 (4)	5% (1%)	50 (6)	7% (1%)
4	22 (6)	3% (1%)	20 (3)	3% (0%)
6	24 (7)	3% (1%)	19 (5)	3% (1%)
7	33 (7)	5% (1%)	37 (4)	5% (1%)
8	39 (4)	5% (1%)	43 (4)	6% (1%)
9	24 (4)	3% (1%)	26 (6)	4% (1%)
10	25 (3)	4% (0%)	22 (4)	3% (1%)
11	23 (5)	3% (1%)	29 (2)	4% (0%)
Grand Mean	28 (7)	4% (1%)	30 (11)	4% (1%)

Handlebar Forward/Rearward Forces

The maximum FR handlebar forces were about half that of the vertical force and ranged from 24N (3N) to 54N (4N), with a grand mean of 40N (9N) on the right handlebar and 40N (10N) on the left. The FR handlebar force values were equivalent to 6% (1%) of the subject's body weight on either handlebar and were always directed forward (away from the subject) on the cycle.

Table 27: Maximum FR Handlebar Forces
Positive Values Indicated a Force Directed Towards the Front of the Cycle

Subject	Right FR Force (SD) Newtons	Percent Body Weight (SD)	Left FR Force (SD) Newtons	Percent Body Weight (SD)
0	34 (1)	5% (0%)	28 (2)	4% (0%)
1	26 (3)	4% (0%)	43 (7)	6% (1%)
3	33 (3)	5% (0%)	46 (2)	7% (0%)
4	46 (2)	6% (0%)	53 (2)	7% (0%)
6	31 (5)	4% (1%)	24 (3)	4% (0%)
7	43 (3)	6% (0%)	39 (3)	5% (0%)
8	50 (4)	7% (1%)	39 (4)	5% (0%)
9	54 (4)	8% (1%)	49 (3)	7% (0%)
10	42 (5)	6% (1%)	29 (4)	4% (1%)
11	42 (1)	5% (0%)	51 (2)	6% (0%)
Grand Mean	40 (9)	6% (1%)	40 (10)	6% (1%)

75

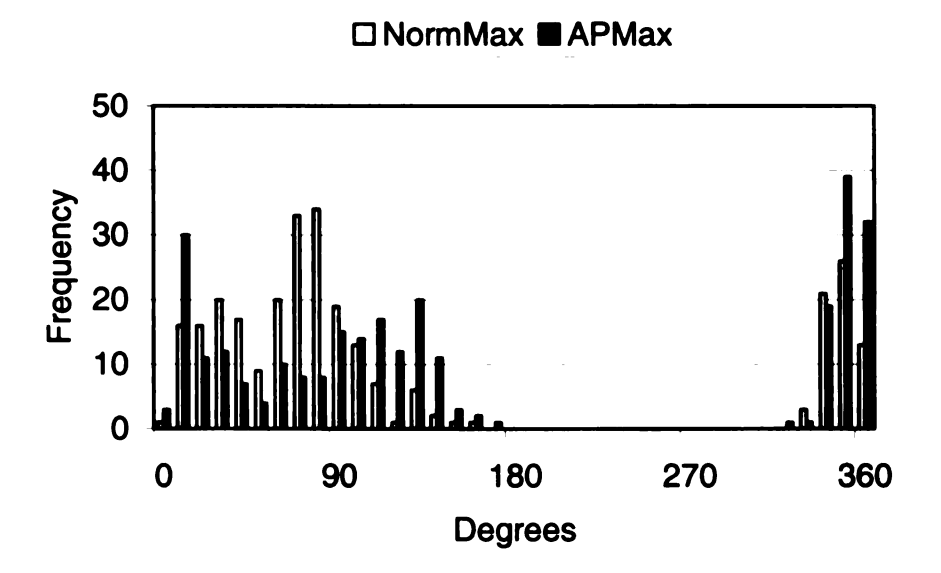
The timing angles for the maximum FR handlebar forces varied across subjects and ranged from -16° (5°), or 344° (5°), to 103° (61°) for the right handlebar, and 170° (26°) to 261° (48°) for the left handlebar. The grand mean timing angle for the maximum FR handlebar forces was 48 (58) for the right handlebar and 212 (48) for the left handlebar.

Table 28: Timing Angle of the Maximum FR Handlebar Force

Subject	Right Handlebar Angle ^o (SD)	Left Handlebar Angle ^o (SD)
0	-5 (18)	187 (24)
1	74 (47)	231 (48)
3	58 (38)	227 (44)
4	103 (61)	253 (29)
6	66 (34)	223 (27)
7	18 (56)	170 (26)
8	93 (45)	172 (22)
9	-16 (5)	205 (65)
10	63 (72)	261 (54)
11	23 (37)	190 (27)
Grand Mean	48 (58)	212 (48)

The timing angle data for the maximum vertical and FR right handlebar forces were plotted together according to their frequency of occurrence, Figure 26. No clear

Figure 26: Frequency of Right Maximum Vertical and FR Handlebar Timing Angles



of approximately 100°. Although not shown, a similar pattern occurred for the left handlebar forces, which would have filled in the remainder of the angles between 180° and 360°.

The minimum FR handlebar forces ranged from 10N (4N) to 30N (3N) on the right handlebar and 9N (2N) to 32N (3N) on the left handlebar, with a grand mean of 20N (7N) and 19N (8N) respectively, as shown in Table 29. The FR handlebar force grand means were equivalent to 3% (1%) BW on both the right and left handlebars and were always oriented in the anterior (forward) direction on the cycle.

Table 29: Minimum FR Handlebar Forces;
Positive values indicated that the forces were directed forward on the cycle

Subject	Right FR Force (SD) Newtons	Percent Body Weight (SD)	Left FR Force (SD) Newtons	Percent Body Weight (SD)
0	18 (2)	3% (0%)	9 (2)	1% (0%)
1	10 (4)	1% (1%)	22 (4)	3% (1%)
3	12 (3)	2% (0%)	18 (4)	3% (1%)
4	26 (3)	3% (0%)	32 (3)	4% (0%)
6	17 (3)	2% (0%)	11 (2)	2% (0%)
7	18 (5)	2% (1%)	10 (4)	1% (1%)
8	28 (2)	4% (0%)	19 (5)	3% (1%)
9	30 (3)	4% (0%)	28 (2)	4% (0%)
10	19 (4)	3% (1%)	12 (2)	2% (0%)
11	22 (2)	3% (0%)	27 (3)	3% (0%)
Grand Mean	20 (7)	3% (1%)	19 (8)	3% (1%)

The timing angle for the minimum right handlebar FR force ranged from 196° (27°) to 269° (6°) and had a grand mean of 240° (27°). For the left handlebar, the timing angle ranged from 42° (34°) to 77° (57°), with a grand mean of 55° (28°). The standard deviations of the grand means (27° for the right, 28° for the left) were similar to those reported for the minimum handlebar vertical loads, and were approximately 8% of the full crank arm revolution.

Table 30: Minimum Handlebar FR Force Timing Angles

Subject	Right Handlebar Angle° (SD)	Left Handlebar Angle ^o (SD)
0	196 (27)	65 (10)
1	243 (29)	77 (57)
3	238 (27)	59 (16)
4	248 (13)	50 (13)
6	257 (30)	47 (11)
7	234 (9)	46 (10)
8	246 (18)	42 (34)
9	238 (14)	47 (27)
10	229 (16)	45 (22)
11	269 (6)	71 (26)
Grand Mean	240 (27)	55 (28)

The range between the maximum and minimum handlebar FR forces varied from 14N (4N) to 25N (5N) on the right handlebar and 14N (3N) to 29N (3N) on the left handlebar, with grand means of 20N (5N) and 21N (5N), respectively. The ranges between the maximum and minimum handlebar FR forces varied from 2-3% on the right handlebar and 2-4% on the left handlebar, with grand means equivalent to 3% (1%) of BW on both the right and left handlebars.

Table 31: Range between the Maximum and Minimum FR Handlebar Forces

Subject	Right FR Force (SD) Newtons	Percent Body Weight (SD)	Left FR Force (SD) Newtons	Percent Body Weight (SD)
0	16 (2)	2% (0%)	19 (2)	3% (0%)
1	17 (3)	2% (0%)	21 (5)	3% (1%)
3	21 (3)	3% (0%)	27 (4)	4% (1%)
4	21 (4)	3% (1%)	21 (3)	3% (0%)
6	14 (4)	2% (1%)	14 (3)	2% (0%)
7	25 (5)	3% (1%)	29 (3)	4% (0%)
8	21 (2)	3% (0%)	19 (3)	3% (0%)
9	24 (4)	3% (1%)	21 (3)	3% (0%)
10	23 (4)	3% (1%)	18 (3)	3% (1%)
11	20 (2)	3% (0%)	24 (2)	3% (0%)
Grand Mean	20 (5)	3% (1%)	21 (5)	3% (1%)

Handlebar Lateral Forces

The right and left maximum lateral handlebar forces were the smallest handlebar forces measured. These forces were not calculated as a percentage of body weight (%BW), as the result would have been less than 1% in most cases. Insufficient data was collected on the left handlebar lateral forces for Subject 0 and were not included in this analysis. Similar to the lateral pedal and seat data, positive values indicate a force

directed towards right lateral, and negative values indicate forces directed towards left lateral.

The maximum values of the lateral right handlebar force ranged from 5N (1N) to 20N (1N) and had a grand mean of 13N (1N), while the left handlebar ranged from -2N (2N) to -16N (1N) and had a grand mean of -9N (5N). The maximum forces measured on the right handlebar were directed right laterally as indicated by their positive value, while the negative values on the left handlebar were directed left laterally.

Table 32: Maximum Lateral Handlebar Forces
Positive Force Values Indicated Forces Directed Right Lateral,
Negative Values Indicated Forces Directed Left Lateral

Subject	Right Lateral Force Newtons (SD)	Left Lateral Force Newtons (SD)
0	6 (1)	-
1	5 (1)	-5 (3)
3	16 (2)	-16 (1)
4	15 (1)	-10 (1)
6	10 (3)	-2 (2)
7	14 (1)	-3 (1)
8	16 (2)	-9 (1)
9	20 (1)	-15 (2)
10	14 (1)	-8 (2)
11	15 (1)	-14 (1)
Grand Mean	13 (5)	-9(5)

The timing angles of the maximum handlebar lateral forces ranged from 7° (25°) to 79° (23°) on the right handlebar and had a grand mean of 50° (41°), while on the left handlebar the timing angles ranged from 181° (41°) to 257° (13°) with a grand mean timing angle of 226° (51°).

Table 33: Maximum Handlebar Lateral Force Timing Angles

Subject	Right Handlebar Angle° (SD)	Left Handlebar Angle° (SD)
0	7 (25)	•
1	75 (47)	200 (104)
3	65 (25)	230 (19)
4	46 (40)	251 (7)
6	75 (35)	219 (74)
7	19 (17)	181 (41)
8	79 (23)	231 (26)
9	65 (34)	250 (6)
10	26 (49)	257 (13)
11	44 (33)	220 (36)
Grand Mean	50 (41)	226 (51)

The minimum lateral handlebar forces, again directed right laterally with positive values and left laterally with negative values, were the smallest forces measured in this analysis. The minimum lateral right handlebar forces ranged from -3N (3N) to 9N (2N) with a grand mean of 2N (4N). On the left handlebar, the minimum lateral forces ranged from -5N (1N) to 4N (2N) with a grand mean 1N (4N).

Two of the subjects minimum force values on the right handlebar switched direction (from right to left lateral) compared to the maximum value, one had a zero minimum force value, and seven continued to load the handlebar towards right lateral.

Five of the subject's minimum force values on the left handlebar were directed right laterally, one went to zero, and two subjects force values remained directed left laterally.

Table 34: Minimum Lateral Handlebar Forces
Positive Force Values Indicated Forces Directed Right Lateral,
Negative Values Indicated Forces Directed Left Lateral

Subject	Right Lateral Force Newtons (SD)	Left Lateral Force Newtons (SD)
0	-1 (1)	
1	-3 (3)	4 (2)
3	0 (1)	0 (1)
4	2 (3)	0 (1)
6	1 (3)	4 (1)
7	2 (1)	4 (1)
8	3 (2)	2 (1)
9	9 (2)	-5 (1)
10	4 (1)	1 (2)
11	5 (1)	-5 (1)
Grand Mean	2 (4)	1(4)

83

The timing angles of the minimum lateral handlebar forces ranged from 225° (12°) to 274° (8°) and had a grand mean of 252° (26°) on the right handlebar. The timing angle of the minimum lateral handlebar forces ranged from 29° (36°) to 79° (22°) on the left handlebar, with a grand mean of 49° (38°).

Table 35: Minimum Lateral Handlebar Force Timing Angles

Subject	Right Handlebar Angle° (SD)	Left Handlebar Angle° (SD)
0	253 (19)	••
1	264 (43)	65 (69)
3	253 (6)	60 (17)
4	245 (18)	32 (25)
6	267 (35)	79 (22)
7	232 (19)	46 (33)
8	250 (22)	49 (33)
9	263 (6)	44 (24)
10	225 (12)	34 (39)
11	274 (8)	29 (36)
Grand Mean	252 (26)	49 (38)

The range between the maximum and minimum handlebar lateral forces varied from 7N (1N) to 16N (2N), with a grand mean of 11N (3N) on the right handlebar. For the left handlebar, the range again varied between 7N (1N) and 16N (1N), with a grand mean of 10N (3N). Data was incomplete for the left handlebar in all tests performed by Subject 0.

Table 36: Range between the Magnitude of the Maximum and Minimum Handlebar Lateral Forces

Subject	Right Lateral Force Range Newtons (SD)	Left Lateral Force Range Newtons (SD)
0	7 (1)	••
1	8 (3)	9 (4)
3	16 (2)	16 (1)
4	13 (3)	9 (2)
6	9 (2)	7 (2)
7	12 (2)	7 (1)
8	13 (1)	11 (1)
9	11 (2)	10 (2)
10	11 (1)	9 (2)
11	10 (2)	9 (1)
Grand Mean	11 (3)	10 (3)

Significant Effects due to Changes in Handlebar Position

The force and timing angle values presented in the previous section were for the Regular handlebar position. In this section of Results, statistical comparisons of the measures recorded in the Regular handlebar position were made to those obtained from the Close and Far handlebar positions. In all, the grand means of 43 force and timing angle measures each were compared for the seat and handlebars, as well as 17 measures of the pedal forces. These included maximum and minimum forces, timing angles of the maximum and minimum forces, and ranges between the maximum and minimum forces. The null hypothesis was that zero differences existed in the grand means of the measures across all subjects with a change in handlebar position.

At a confidence interval of 95% (level of significance α =0.05), there would be a high probability that a change in handlebar position affected a measure for those values where P<0.05. For this analysis however, any measure that had a value of P<0.15 between at least two of the handlebar positions tested were included in the tables that follow, on the basis that further study may be needed to clarify a relationship between that measure and the change in handlebar position.

Pedal Measures

Of the 17 different measures observed from the pedal loads, three of the force values were significantly affected (P < 0.05) in at least one change of the handlebar position, i.e. from Close-Far, Close-Regular, or Far-Regular, Table 37below. The maximum tangent force to left crank arm path was nearly significant from Close-Regular and Far-Regular, with P = 0.078 and 0.0870 respectively, Table 38.

Table 37: Mean Pedal Forces That Showed a Statistically Significant Difference at P < 0.15 for at Least One Handlebar Position Change, i.e. Close-Far, Close-Regular, or Far- Regular

Measure	Close Position Force (SE) Newtons	Regular Position Force (SE) Newtons	Far Position Force (SE) Newtons
Max Left Tangent to Crank Arm Path	180.0 (6.8)	172.8 (6.6)	179.3 (6.6)
Max Left Pedal Lateral	-40.6 (2.9)	-38.2 (2.8)	-40.8 (2.8)
Min Left Pedal Lateral	6.2 (1.1)	7.2 (1.1)	6.7 (1.1)
Min Right Pedal Lateral	-3.8 (0.8)	-5.0 (0.8)	-4.0 (0.8)

Table 38: Probability of Zero Difference in Pedal Forces
With a Change in Handlebar Position;
P<.05 indicated with Bold Font
P<.15 indicated with *

Measure	Close- Far P=	Close- Regular P =	Far- Regular P =
Max Left Tangent to Crank Arm Path	0.8506	0.0778*	0.0870*
Max Left Pedal Lateral	0.8520	0.0428	0.0163
Min Left Pedal Lateral	0.2784	0.0252	0.2056
Min Right Pedal Lateral	0.6457	0.0178	0.0373

Table 39: Pedal Force Timing Angles That Showed a Statistically Significant Difference of P < 0.15 for at Least One Handlebar Position Change, i.e. Close-Far, Close-Regular, or Far-Regular

Measure	Close Position Angle ° (SE)	Regular Position Angle ° (SE)	Far Position Angle ° (SE)
Max Left Tangent to Crank Arm Path	103.2 (3.3)	104.4 (3.3)	102.1 (3.3)
Min Left Tangent to Crank Arm Path	277.6 (2.3)	281.4 (2.1)	277.0 (2.1)

Table 40: Probability of Zero Difference in Pedal Force Timing Angles
With a Change in Handlebar Position;

P<.05 indicated with Bold Font

P<.15 indicated with *

Measure	Close- Far P =	Close- Regular P =	Far- Regular P=
Max Left Tangent to Crank Arm		i	
Path	0.4234	0.4053	0.0767*
Min Left Tangent to Crank Arm			
Path	0.8294	0.1209*	0.0573*

Seat Measures

The seat forces affected by change in the handlebar position are shown in Table 41 below, and are also presented in terms of percent body weight (%BW) in Table 42. All measures with force values significantly affected by a change in handlebar position were also affected in terms of %BW.

Table 41: Mean Seat Forces That Showed a Statistically Significant Difference at P < 0.15 for at Least One Handlebar Position Change, i.e. Close-Far, Close-Regular, or Far-Regular

Measure	Close Position Force (SE) Newtons	Regular Position Force (SE) Newtons	Far Position Force (SE) Newtons
Max Seat Vertical 0-180	-353.3 (17.6)	-368.7 (17.9)	-371.7 (17.5)
Max Seat Vertical 180-360	-358.5 (14.9)	-363.6 (14.8)	-368.3 (14.8)
Min Seat Vertical 0-180	-284.6 (15.9)	-291.7 (15.7)	-291.5 (15.8)
Min Seat Vertical 180-360	-284.7 (14.6)	-291.5 (14.5)	-295.5 (14.5)
Max Seat FR 0-180	-77.9 (5.8)	-77.9 (5.7)	-83.1 (5.7)
Max Seat FR 180-360	-78.4 (6.1)	-78.6 (6.1)	-85.2 (6.1)
Min Seat FR 0-180	-40.0 (6.2)	-39.2 (6.1)	-43.3 (6.1)
Min Seat FR 180-360	-41.0 (6.2)	-39.4 (6.1)	-43.9 (6.1)
Range of Max and Min FR Forces	37.4 (3.2)	39.2 (3.1)	41.3 (3.1)

Table 42: Mean Seat Forces in %BW that showed a Statistically Significant Difference of P< 0.15 for at Least One Handlebar Change, i.e. Close-Far, Close-Regular, or Far-Regular

Measure	Close Position % BW (SE)	Regular Position %BW (SE)	Far Position %BW (SE)
Max Seat Vertical 0-180°	49.3% (1.8%)	51.4% (1.8%)	51.8% (1.8%)
Max Seat Vertical 180-360°	50.0% (1.4%)	50.7% (1.3%)	51.3% (1.3%)
Min Seat Vertical 0-180°	39.7% (1.8%)	40.7% (1.8%)	40.6% (1.8%)
Min Seat Vertical 180-360°	39.7% (1.6%)	40.7% (1.6%)	41.2% (1.6%)
Max Seat FR 0-180°	10.8% (0.8%)	11.0% (0.8%)	11.6% (0.8%)
Max Seat FR 180-360°	10.9% (0.8%)	11.0% (0.8%)	11.9% (0.8%)
Min Seat FR 0-180°	5.6% (0.9%)	5.5% (0.9%)	6.1% (0.9%)
Min Seat FR 180-360°	5.7% (0.9%)	5.5% (0.9%)	6.2% (0.9%)

Table 43: Probability of Zero Difference in Seat Forces
With a Change in Handlebar Position;

P<.05 indicated with Bold Font

P<.15 indicated with *

Measure	Close-Far	Close- Regular P =	Far-Regular P =
Max Seat Vertical 0-180°	0.0013	0.0001	0.4814
%BW Max Seat Vertical 0-180°	0.0012	0.0001	0.4711
Max Seat Vertical 180-360°	0.0117	0.1844	0.1898
%BW Max Seat Vertical180-360°	0.0117	0.1755	0.1999
Min Seat Vertical 0-180°	0.1519	0.1429*	0.9716
%BW Min Seat Vertical 0-180°	0.1754	0.1499*	0.9261
Min Seat Vertical 180-360°	0.0031	0.0604*	0.2311
%BW Min Seat Vertical 180-360°	0.0036	0.0580*	0.2589
Max Seat FR 0-180°	0.0187	0.9753	0.0117
%BW Max Seat FR 0-180°	0.0138	0.9521	0.0090
Max Seat FR 180-360°	0.0016	0.9434	0.0008
%BW Max Seat FR 180-360	0.0015	0.9414	0.0008
Min Seat FR 0-180°	0.1288*	0.7262	0.0425
%BW Min Seat FR 0-180°	0.1163*	0.7633	0.0421
Min Seat FR 180-360°	0.1754	0.4512	0.0223
%BW Min Seat FR 180-360°	0.1519	0.4755	0.0200
Range of Max and Min FR Forces	0.0091	0.2295	0.1224*

Several timing angles for the seat forces showed significant differences with a change in handlebar position, Table 44. It was stated previously in the Results section however, that the grand mean timing angles of the maximum seat vertical forces could not be confirmed. These results were presented here for completeness, but should be considered carefully.

Table 44: Mean Seat Force Timing Angles That Showed a Statistically Significant Difference of P < 0.15 for at Least One Handlebar Position Change, i.e. Close-Far, Close-Regular, or Far-Regular

Measure	Close Position Angle ° (SE)	Regular Position Angle ° (SE)	Far Position Angle ° (SE)
Max Seat Vertical Angle 0-180°	113.6 (11.1)	108.5 (10.8)	92.8 (10.8)
Max Seat Vertical Angle 180-360°	265.6 (13.3)	288.5 (13.0)	283.1 (13.0)
Max Seat FR Angle 180- 360°	269.2 (5.6)	267.5 (5.4)	275.4 (5.4)
Max Seat Lateral Angle 0-180°	102.3 (9.9)	92.0 (9.6)	102.9 (9.6)
Max Seat Lateral Angle 180-360°	269.4 (9.3)	266.2 (9.1)	260.6 (9.1)

Table 45: Probability of Zero Difference in Seat Force Timing Angles
With a Change in Handlebar Position;

P<.05 indicated with Bold Font

P<.15 indicated with *

Measure	Close-Far P =	Close-Regular P =	Far-Regular P =
Max Seat Vertical Angle 0-180°	0.0022	0.4533	0.0118
Max Seat Vertical Angle 180-360°	0.0233	0.0032	0.4477
Max Seat FR Angle 180-360°	0.1196*	0.6728	0.0321
Max Seat Lateral Angle 0-180°	0.9241	0.1195*	0.0729
Max Seat Lateral Angle 180-360°	0.088	0.5282	0.2407

Handlebar Measures

Of the 43 measures compared at the right and left handlebars, 13 force values, six %BW values, and eight timing angle values were significantly affected by at least one variation of the handlebar position. Similar to the seat forces mentioned previously, significance was seen in both the handlebar forces and their corresponding expressions terms of %BW.

Table 46: Mean Handlebar Forces That Showed a Statistically Significant Difference at P<0.15 for at Least One Handlebar Position Change, i.e. Close-Far, Close-Regular, or Far-Regular

Measure	Close Position Force (SE) Newtons	Regular Position Force (SE) Newtons	Far Position Force (SE) Newtons
Max Right Vertical	-83.4 (4.1)	-80.0 (4.1)	-81.3 (4.1)
Max Left Vertical	-81.6 (4.6)	-78.5 (4.6)	-78.8 (4.6)
Min Left Vertical	-50.8 (3.1)	-48.3 (3.1)	-46.2 (3.1)
Max Right FR	36.9 (2.8)	40.2 (2.7)	44.1 (2.7)
Max Left FR	38.7 (3.3)	40.1 (3.3)	44.0 (3.3)
Min Right FR	18.1 (1.8)	20.0 (1.8)	20.6 (1.8)
Max Right Lateral	13.4 (1.7)	13.1 (1.6)	14.2 (1.6)
Min Right Lateral	1.4 (1.0)	2.1 (1.0)	2.4 (1.0)
Range of Max and Min Right Vertical	30.3 (2.4)	27.9 (2.3)	30.1 (2.3)
Range of Max and Min Left Vertical	30.8 (3.5)	30.3 (3.5)	32.7 (3.5)
Range of Max and Min Right FR	18.8 (1.5)	20.2 (1.4)	23.5 (1.4)
Range of Max and Min Left FR	20.2 (1.6)	21.3 (1.5)	25.9 (1.5)
Range of Max and Min Right Lateral	12.0 (1.2)	11.0 (1.1)	11.9 (1.1)

Table 47: Mean Handlebar Forces in %BW that Showed a Statistically Significant Difference of P< 0.15 for at Least One Handlebar Change, i.e. Close-Far, Close-Regular, or Far-Regular

Regular, or Tar-Regular			
Measure	Close Position % BW (SE)	Regular Position %BW (SE)	Far Position %BW (SE)
Max Right Vertical	11.6% (0.5%)	11.2% (0.5%)	11.4% (0.5%)
Max Left Vertical	11.4% (0.5%)	11.0% (0.5%)	11.0% (0.5%)
Min Left Vertical	7.1% (0.3%)	6.7% (0.3%)	6.4% (0.3%)
Max Right FR	5.1% (0.4%)	5.6% (0.4%)	6.2% (0.4%)
Max Left FR	5.4% (0.4%)	5.6% (0.4%)	6.1% (0.4%)
Min Right FR	2.5% (0.2%)	2.8% (0.2%)	2.9% (0.2%)

Table 48: Probability of Zero Difference in Handlebar Forces
With a Change in Handlebar Position;

P<.05 indicated with Bold Font

P<.15 indicated with *

Measure	Close-Far P =	Close-Regular P =	Far-Regular P =
Max Right Vertical	0.1939	0.0427	0.4252
%BW Max Right Vertical	0.2211	0.0434	0.3834
Max Left Vertical	0.0234	0.012	0.7862
% BW Max Left Vertical	0.027	0.0123	0.7468
Min Left Vertical	0.0002	0.0414	0.0662*
%BW Min Left Vertical	0.0003	0.0405	0.0734*
Max Right FR	<.0001	0.0161	0.0022
%BW Max Right FR	<.0001	0.0168	0.0021
Max Left FR	<.0001	0.1576	<.0001
%BW Max Left FR	<.0001	0.1613	<.0001
Min Right FR	0.0164	0.0701*	0.5179
%BW Min Right FR	0.0139	0.0705*	0.4738
Max Right Lateral	0.3053	0.7571	0.1478*
Min Right Lateral	0.0876*	0.1993	0.6422
Range of Max and Min Right Vertical	0.8614	0.0516*	0.0538*
Range of Max and Min Left Vertical	0.0822*	0.6141	0.015
Range of Max and Min Right FR	<.0001	0.1432*	0.0002
Range of Max and Min Left FR	<.0001	0.1772	<.0001
Range of Max and Min Right Lateral	0.9077	0.1245*	0.1226*

The timing angles that corresponded to a maximum or minimum force that showed a significant difference due to a change in the handlebar position are shown in Table 49. The timing angle of the maximum right lateral force showed the largest standard error of 13.5° to 14.6° across the three positions, and the P values associated with these measures should be considered carefully.

Table 49: Mean Handlebar Force Timing Angles That Showed a Statistically Significant Difference of P < 0.15 for at Least One Handlebar Position Change, i.e.

Close-Far, Close-Regular, or Far-Regular

	Close	Regular	Far
Measure	Position Angle ° (SE)	Position Angle ° (SE)	Position Angle ° (SE)
Max Right Vertical	Augie (SE)	Augie (SE)	Angle (SE)
Angle	34.9 (7.3)	44.5 (6.8)	42.5 (6.8)
Max Left Vertical			
Angle	212.8 (6.8)	220.9 (6.4)	223.8 (6.4)
Min Right Vertical			
Angle	236.0 (5.3)	229.2 (5.1)	226.5 (5.1)
Max Left FR Angle	218.2 (9.8)	211.8 (9.3)	224.0 (9.3)
Min Right FR Angle	243.0 (5.6)	239.9 (5.4)	236.0 (5.4)
Min Left FR Angle	58.4 (4.6)	54.9 (4.2)	49.0 (4.2)
Max Right Lateral			
Angle	86.1 (14.6)	107.6 (13.5)	114.1 (13.5)
Min Right Lateral			
Angle	243.6 (4.9)	252.5 (4.5)	235.6 (4.5)

Table 50: Probability of Zero Difference in Handlebar Force Timing Angles
With a Change in Handlebar Position;
P<.05 indicated with Bold Font

.05 indicated with Bold Font

P< .15 indicated with *

Measure	Close-Far <i>P</i> =	Close-Regular P =	Far-Regular P =
Max Right Vertical Angle	0.2394	0.1400*	0.7446
Max Left Vertical Angle	0.0461	0.1413*	0.5667
Min Right Vertical Angle	0.0277	0.1157*	0.4903
Max Left FR Angle	0.4548	0.4062	0.0877*
Min Right FR Angle	0.069*	0.4212	0.2687
Min Left FR Angle	0.061*	0.4804	0.2066
Max Right Lateral Angle	0.0599*	0.1467*	0.6396
Min Right Lateral Angle	0.0793*	0.0529*	<.0001

Discussion and Conclusions

Baseline Rider/Cycle Interface Seat and Handlebar Forces

On the premise that skin, groin, and other non-traumatic cycling injuries may be the result of combined loading at the rider/cycle interfaces, the first goal of this research was to describe the baseline vertical and shear force values at the rider/cycle interfaces. Also evaluated were the corresponding timing angles (the left crank arm angles at which the maximum and minimum forces occurred). Both the forces and timing angles were measured for a bicycle fitting approach commonly used in commercial settings to properly adjust the bicycle handlebars at the correct reach from the seat.

Seat Forces

During a single crank arm revolution, the data support the conclusion that consistent loading was applied to the groin region during all of the cycling tests. For example, the vertical and forward/rearward (AP) shear forces were never zero, and both exhibited a cyclical profile that cycled between the maximum and minimum forces (always negative magnitudes) twice per crank arm revolution. This indicated that the vertical forces always acted in the downward direction and the FR forces acted in the rearward direction on the cycle. This finding supported two other pieces of work, and also described the double cycle of these forces. Bolourchi and Hull (1985) described the profile of the measured force along the axis of the bicycle seat tube as reactive to the pedal loads for three subjects, which displayed a "double cycle" profile for every crank arm revolution, one attributed to each legs contribution to driving the crank arms of the

cycle. Stone and Hull (1995) also noted a similar pattern with the measured FR seat force in tests of five subjects.

In contrast to the vertical and FR seat forces the lateral, or side to side, seat shear forces were relieved once per crank arm revolution and displayed a "single cycle" force profile, as the force magnitude went to zero and then switched direction from left lateral to right lateral. As the left leg drove the crank arms the positive force magnitude on the seat indicated the lateral shear force was directed to the right on the cycle, or to the left on the subject. Similarly, when the right leg was driving the negative force magnitudes indicated the forces were directed to the left on the cycle or to the right on the subject. This suggested that the lateral seat forces were related to the pedal reaction forces.

The grand mean of the vertical seat forces alternated between a minimum of 41% of the subjects' body weight (% BW) (292N, standard deviation (SD) 49N) and a maximum 52% BW (372N (56N)) in the Regular position. As expected, the vertical seat forces were the largest measured forces at any of the rider/cycle interfaces. Presented in the Introduction, other authors have theorized these forces were directly related to groin injuries such as occluding blood and oxygen flow to the surface of the skin and other internal body parts, nerve entrapment, bruising, skin ulceration, and erectile dysfunction.

The maximum vertical forces expressed in %BW found during cycling were lower than those found under the buttocks of subjects in other seated postures (i.e. office chairs or automobile seats). Bush (2000) showed that approximately 53-56% of a subject's body weight was supported by the buttocks, and was dependant on the subject's position in the chair. This is an interesting finding, as non-traumatic injuries attributed to cycling (bruising, perineal and genital numbness, impotence, "accessory testicles") are

generally not experienced by individuals in other seated postures. This likely resulted from many differences between the two postures, which included contact area between the seat and subject, temperature, and moisture. Another factor that should be considered was the cyclical nature of the shear forces in cycling. Also, unique to the cycling posture the body weight was partially supported in the anterior areas of the groin (the perineum) in addition to the buttocks, as contact was consistently shown through mapped pressure data in this region.

Shear forces have been mentioned in literature as secondary causative factors in non-traumatic skin injury, but until now were overlooked in terms of quantitative data. The seat shear forces acting in the forward/rearward (FR) direction alternated between 5% and 11% BW (39N (22N) to 78N (20N)), and were always directed forwards on the groin of the rider. Similar to the vertical seat forces, the FR shear forces were consistently negative throughout the crank arm revolution, never reached zero, and were directed rearward on the cycle. As such, the FR shear continuously pushes the tissue of the groin forward, and Bennett et al. (1979) described the respective compressive and tensile states of the tissue immediately forward and rearward of the contact zone. In their work, Bennett et al. also pointed to the fact that both of these tissue states acted to resist motion at the contacting surfaces, so their measurement device likely registered less force than was actually present in the tissues immediately forward and rearward of the contact zone. Though they explained acceptably small amounts of error for their test condition, they also postulated that larger force value errors (i.e. larger forces in the tissue than actually measured) would be present in data obtained testing skin over bony prominences than over muscle mass. Making a similar comparison in the cycling activity (i.e. with the skin of the groin pressed into the bony prominences of the pelvis) the shear force magnitudes in the skin of the groin adjacent to its contact zones with the seat may have been larger than were measured.

In contrast to the FR seat forces, the lateral seat forces reached their maximum magnitudes and then were momentarily relieved in the transition between the periods of the left and right leg driving the crank arms of the cycle. The lateral force magnitudes reached maximums of 4% to 5% BW (31N (8N) to 33N (8N)), and were always directed away from the driving leg on the cycle.

As discussed in the Results, two different lateral seat force profiles were observed among the subjects tested. Six subjects displayed a "double hump" profile, while four displayed a "single hump" profile. Generally, the subjects who displayed the "double hump" profile had standard deviations in their timing angles much greater than those that displayed the "single hump" profile. However, this was expected after it was noticed that the larger force magnitude could have occurred at either the first or second "hump". While this difference was noted, no inferences were made as to causal factors between the subjects that displayed one profile or the other. One possibility for the difference seen in the force profiles may have been related to a subject's efficiency in producing power around the crank arm revolution. Another explanation may have been that the different profiles were somehow related to muscle activation and coordination differences between subjects.

It was recognized that the measured magnitudes of the seat shear forces were a fraction (approximately 10% to 20%) of the vertical force magnitudes, but their secondary contribution in occluding blood flow to the surface of the skin in the palm has

been examined. Bennett et al (1979) found that when exposed to shear stress values of approximately 0.981 N/cm² (100 g/cm²), only half the magnitude of normal pressure (compared to the no shear stress condition) was necessary to occlude blood flow. Based on this, a reduction in the magnitudes of the shear forces at the rider/seat interface could delay the onset and decrease the severity or occurrence of non-traumatic skin injuries at the groin. These forces may be under one's control to manage through the design and shape of the seat, or through changes to the seat and handlebar position. Perhaps future work could assess the shear force values between different seat designs, for example those with cutouts and those without.

Handlebar Forces

Maximum and minimum handlebar forces were collected from the right and left hand once per crank arm revolution as the vertical, FR shear, and lateral shear forces at the handlebars exhibited a single cycle force profile per crank arm revolution. This finding was in contrast to the force profiles reported by Bolourchi and Hull (1985) and Stone and Hull (1995), but their handlebar force data included the contributions from both hands through a single dynamometer. To this author's knowledge, the interface forces measured individually at the right and left hands has not been previously reported.

Each of the hands supported vertical forces that ranged between a minimum of 7% BW (approximately 50N (12N)) and a maximum 11% BW (80N (15N)) averaged across all of the subjects, and a FR shear force that ranged from 3% to 6% BW (20N (8N) to 40N (10N)). The vertical forces were always directed on the handlebars towards the ground, and the FR forces were always directed towards the front of the cycle. Thus the vertical forces acted upwards and FR forces acted rearwards on the hands of the subject.

An aspect of the handlebar loading that has not been previously reported was the asymmetrical loading shown between the right and left handlebar forces in several subjects. Subjects 0, 6, 7, and 8 placed considerably (>15%) more load on the right hand than the left, and subjects 1, 3, and 11 consistently placed more load on their left hand. This asymmetrical loading may be due to various musculoskeletal imbalances, such as in the back, pelvis, shoulders, and arms. Also, the difference in loading may be necessary for balance as the loads transfer between all of the interfaces. A more involved investigation of the kinematics of the rider's body may provide further insight into this observation.

The lateral handlebar forces had the smallest magnitudes, and were typically less than 1% BW. The mean lateral forces magnitudes ranged from a minimum of 1N to a maximum of 13N across the ten subjects tested, and were reported here merely for completeness of the data set.

Timing Angles

The grand mean timing angles for the minimum vertical seat force occurred in the regions near 0° and 180° for the ten subjects tested. This confirmed the timing angle data presented by Bolourchi and Hull (1985) for their three subjects.

The grand mean timing angles for the maximum vertical seat forces were 108° and 288° during their respective portions of the crank arm revolution (i.e. 0-180° or 180-360°). While the mean timing angles were consistent for the most part within a set of tests for a subject, they ranged approximately 100° amongst the ten subjects while either the right or left leg was driving the crank arm. This resulted in standard deviations (SD) for the grand mean timing angles of 38° and 45°, respectively.

A finding that was not immediately intuitive was the region of contact between the rider and seat at the timing angle of the maximum vertical seat forces. Mapped pressure data showed that the pelvis and buttock region opposite to that of the driving leg was fully or primarily in contact with the seat rather than the same side. This finding supported conclusions by Bolourchi and Hull (1985). Bolourchi and Hull theorized this phenomenon from their evaluation of the moment profiles reactive to vertical loads on the seat, and they attributed it to increased body weight being supported by the pedal of the driving leg at the bottom of its pedal stroke.

At first glance, comparison of the timing angles indicated the vertical seat forces while may have occurred as a reaction to the forces tangent to the left crank arm path, as they both occurred near the same timing angles. After looking at the standard deviations of the timing angles in both cases however, those of the maximum and minimum forces tangent to the crank arm path were more regular than those of the maximum and minimum vertical seat forces. Therefore, it was theorized that the vertical seat forces were more complicated than being simply reactions to the pedaling forces at the feet, and that force contributions from the hands, as well as the kinematics of the rider's body, may also play a role.

The similarity of the mean timing angles of the vertical (44° (44°)) and FR handlebar forces (48° (58°)) indicated that they generally occurred together. However, with standard deviations equal to approximately one third of their respective regions of occurrence (i.e. 0-180° or 180-360°), further work is needed to verify this finding. If in fact they do occur together, it is possible that the magnitudes of these combined forces would be sufficient to cause injuries to the tissue of the hand or wrist (nerve compression,

tingling of the hands, swelling of the compartments of the wrist), especially if they were highly localized to one region of the hand. This could be problematic if the hands were left in one position for an extended amount of time, for example in the drop rather than the top section of the handlebars or the brake hoods. In future work, pressure mapping at the handlebars would be useful to estimate regions of localized contact that occurs between the hand and handlebar.

Significant Effects from Changes to Handlebar Position

The second goal of this work was to determine if changing the rider's position (through a change in the distance from the seat to the handlebars) significantly affected the interface forces and/or their timing angles.

The minimum and maximum vertical seat forces in this investigation were significantly affected by changes in the length from the seat to the handlebars. More of the body weight was bourn by the seat as the handlebars were moved further away from the seat. This finding did not seem intuitive, as it was expected that more of the subject's weight would be supported at the seat as the body was brought into a more upright riding position through adjustment of the handlebars closer to the seat.

Movement of the handlebars from the closest to the furthest handlebar position resulted in the minimum vertical seat forces increasing from approximately 40% BW to 41% BW and the maximum vertical seat forces increasing from 49% BW to 52% BW. While the minimum vertical seat forces increased approximately 1% BW with a position change, the maximum forces increased approximately 3%. This resulted in an increased range between the minimum and maximum forces as the handlebars were moved away from the subject. The increased range between the forces must also be considered as a

factor in non-traumatic injuries, especially with increased time on the bicycle. For example, at the tested pedaling frequency of 75 RPM the forces cover this range of force magnitudes approximately 9,000 times in a 30-minute ride, since the seat forces cycle twice per complete crank arm revolution.

The FR seat forces were also significantly affected by the change in handlebar position. The maximum FR seat forces increased from 10.8% BW to 11.9% BW as the handlebars were moved from the closest to the furthest handlebar position. The minimum FR seat forces also increased from 5.5% to 6.2% BW, but the ranges between the maximum and minimum force magnitudes were similar across all handlebar positions.

The vertical and FR handlebar forces were also significantly affected by the change in handlebar position, though not as much nor as clearly as the vertical and FR seat forces. Both the right and left handlebar vertical forces significantly decreased from 12% BW to 11% BW with the change from the Close to the Regular position, but no further decrease was noted as the handlebars were moved to the Far position. The FR forces at each handlebar also increased significantly approximately 0.5% BW with every change in handlebar position (i.e., from 5% BW in the Close position to 6% BW in the Far position).

The postures a bicyclist assumes have shown to affect the shape of the lumbar spine, inverting its natural physiological (concave and lordotic) shape, and possibly changing the loading characteristics of the discs (Usabiaga et al. 1997). Although there is some adjustability to the height of the handlebars relative to the seat, changing the reach is a costly proposal. Consumers must purchase a different length stem to properly adjust

reach to the handlebars. With only a limited range of stems lengths available, adjustability of 5cm in either direction of a factory installed stem are about the maximum adjustment available before changing to a different frame size.

The seat of a standard bike allows for adjustment both vertically and fore/aft without the need to purchase additional parts. Biomechanical studies have indicated preferred seat height data for efficient pedaling mechanics, optimized power output, and the prevention of joint injury. For bicyclists with the seat height adjusted for appropriate pedaling mechanics, any changes in the interface force distributions between the seat, handlebars, and pedals may necessitate changes to the reach or relative height of the handlebars to the seat.

The data presented here are the first of their kind, and support the conclusion that moving the handlebars closer to the seat significantly decreases vertical and FR shear loading on the seat. Also, the vertical forces at the handlebars significantly increased, while the FR forces decreased, as the handlebars were moved closer to the seat. It is expected that this information will be useful in the development of future bicycle seats and handlebars, as well as assist bicycle fit experts in positioning riders on their bicycles to reduce the occurrence and severity of non-traumatic injuries related to bicycling.

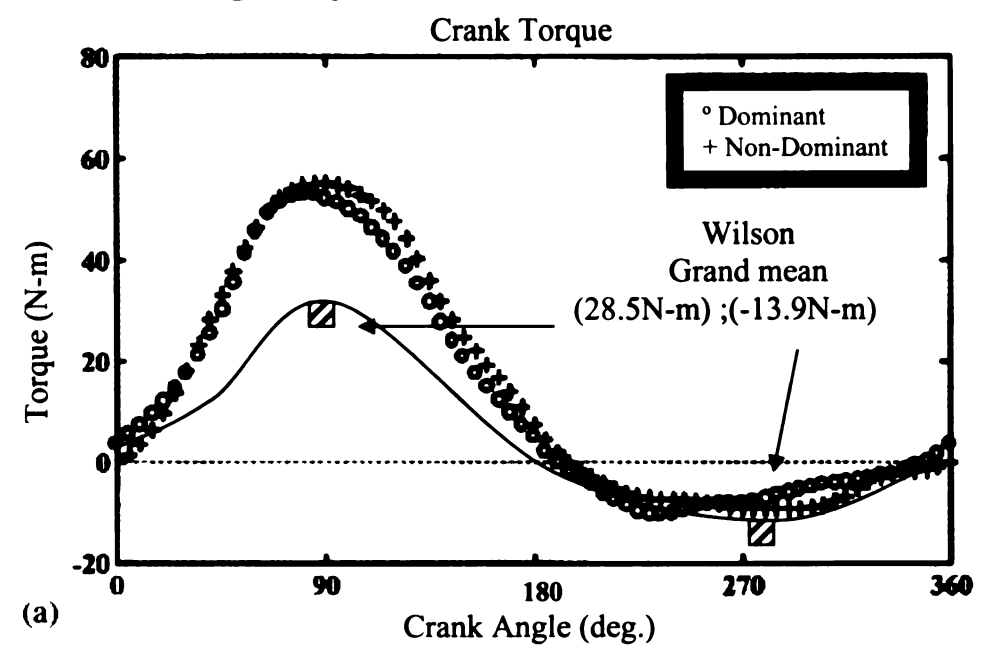
Pedal Data Comparisons

Finally, pedal forces and timing angles were collected for comparisons with research performed by other authors. For the work presented here, timing angles were referenced to the angle of the left crank arm as viewed from the left side of the cycle, where a value of 0° indicated the left pedal was at its highest position in the y-z plane during a crank arm revolution, and 180° indicated its lowest position. Mean (average)

maximum and minimum force values, along with their corresponding timing angles, were calculated from ten complete cycles of force data as described by ten complete revolutions of the crank arm.

Both the maximum and minimum left pedal force component tangent to the crank arm path occurred at timing angles that were in a range consistent with previous research (Neptune et al. 1999, Smak et al. 1999). Previously described in terms of crank torque (N-m) rather than force tangent to the crank arm path (N), the difference was a scalar multiplier of the crank arm length, as shown in Figure 27.

Figure 27: Representative Crank Torque Profile for One Crank Revolution in a Single Subject; Smak et al. (1999), Figure 1(a)



Measured forces at the pedals were a combination of inertial effects from the weight and movement of the legs, as well as muscular contributions from the legs, buttocks, and lower back. When averaged across all subjects, the applied maximum force of 173N (or 28.5N-m of torque with 165mm crank arms) tangent to the path ascribed by the left crank arm occurred at a timing angle of approximately 104°, while a minimum applied force of –84N (-13.9N-m torque) occurred at approximately 281°. The maximum torque magnitudes were approximately half of those reported by Smak et al. (1999), but this was expected from differences in the external power output required of the test subjects (250 watts (Smak et al. 1999) vs. 125 watts for this work).

As these forces were perpendicular to the left crank arm, work was done to drive the crank arms when the force values were positive, and work was done against the crank arm during 180-360°. The local coordinate system of the right pedal was not attained in this work but if symmetry were assumed, the right side forces tangent to the crank arm

path reached their maximum values with the left crank arm near 284° and their minimum values with the left crank arm in the region of 101°.

Favorable comparisons to previous work done on the pedaling forces tangent to the crank arm path, as well as their timing angles, suggested that the measurement equipment used in this investigation were adequate for the study of cycling biomechanics. Also, the techniques used during data reduction were also verified. This was important to justify the order of the pedal force coordinate transformations, since they were transformed into different coordinate systems twice.

References

Andersen, K.V., Bovim, G., 1997. Impotence and nerve entrapment in long distance amateur cyclists. Acta Nuerol. Scand. 95, 233-240.

Ashe, M.C., Scroop, G.C., Frisken, P.I., Amery, C.A., Wilkins, M.A., Khan, K.M., 2003. Body position affects performance in untrained cyclists. Br. J. Sports Med. 37, 441-444.

Bailey, M.P., Maillardet, F.J., Messenger, N., 2003. Kinematics of cycling in relation to anterior knee pain and patellar tendonitis. J. Sports Sci. 21, 649-657.

Bennet, L., Kavner, D., Lee, B.K., Trainor, F.A., 1979. Shear vs pressure as causative factors in skin blood flow occlusion. Arch Phys Med Rehabil. 60, 309-314.

Bolourchi, F., Hull, M.L., 1985. Measurement of rider induced loads during simulated bicycling. Int. J. Sports Biomech. 1, 308-329.

Breda, G., Piazza, N., Bernardi, V., Lunardon, E., Caruso, A., 2005. Development of a new geometric bicycle saddle for the maintenance of genital-perineal vascular perfusion. J. Sex. Med. 2, 605-611.

Bressel, E., Cronin, J., 2004. Bicycle seat interface pressure: reliability, validity, and influence of hand position and workload. J. Biomech. 38, 1325-1331.

Bressel, E., Larson, B.J., 2003. Bicycle seat designs and their effect on pelvic angle, trunk angle, and comfort. Med. Sci. Sports Exerc. 35, 327-332.

Bush, T.R., 2000. Posture and force measures of mid-sized men in seated positions. Doctoral Dissertation, Michigan State University.

Capitani, D., Beer, S., 2002. Handlebar palsy-a compression syndrome of the deep terminal (motor) branch of the ulnar nerve in biking. J. Neurol. 249, 1441-1445.

Christiaans, H.H.C.M., Bremmer, A., 1998. Comfort on bicycles and the validity of a commercial bicycle fitting system. App. Erg. 29, 201-211.

Dettori, J.R., Koepsell, T.D., Cummings, P., Corman, J.M., 2004. Erectile dysfunction after a long-distance cycling event: associations with bicycle characteristics. J. Urology 172, 637-641.

De Vey Mestdagh, K., 1998. Personal perspective: in search of an optimum cycling posture. App. Erg. 29, 325-334.

Edsberg, L.E, Mates, R.E., Baier, R.E., Lauren, M., 1999. Mechanical characteristics of human skin subjected to static versus cyclic normal pressures. J. Rehab. Res. and Dev. 36, 133-141.

Foss, O., Hallen, J., 2005. Cadence and performance in elite cyclists. Eur. J. Appl. Physiol. 93, 453-462.

Gregersen, C.S., Hull, M.L., 2003. Non-driving intersegmental knee moments in cycling computed using a model that includes three-dimensional kinematics of the shank/foot and the effect of simplifying assumptions. J. Biomech. 36, 803-813.

Hobson, D.A, 1992. Comparative effects of posture on pressure and shear at the body-seat interface. J. Rehab. Res. and Dev. 29, 21-31.

Kohler, P., Utermann, S., Kahle, B., Hartschuh, W., 2000. "Biker's nodule"-the perineal nodular induration of the cyclist. Der Hautarzt 51, 763-765.

Lowe, B.D., Schrader, S.M., Breitenstein, M.J., 2004. Effect of bicycle saddle designs on the pressure to the perineum of the bicyclist. Med. Sci. Sports Exerc. 36, 1055-1062.

Martin, J.C., Spirduso, W.W, 2001. Determinants of maximal cycling power: crank length, pedaling rate and pedal speed. Eur. J. Appl. Physiol. 84, 413-418.

Mellion, M.B., 1996. Bicycling Injuries: Prevention, Diagnosis, and Treatment, in Mellion, M.B., (Ed.), Office Sports Medicine, second ed., Hanley & Belfus, Inc., Philadelphia, pp. 355-374.

Munarriz, R.M., Huang, V., Uberoi, J., Maitland, S., Payton, T., Goldstein, I., 2005. Only the nose knows: Penile hemodynamic study on the perineum-saddle interface in men with erectile dysfunction utilizing bicycle saddles and seats with and without nose extensions. J. Sex. Med. 2, 612-619.

National Center for Health Statistics, 2005. Health, United States, 2005 with Chartbook on Trends in the Health of Americans, Hyattsville, MD.

Nayal, W., Schwarzer, U., Klotz, T., Heidenreich, A., Englemann, U., 1999. Transcutaneous penile oxygen pressure during bicycling. BJU Int. 83, 623-625.

Neptune, R.R., Herzog, W., 1999. The association between negative muscle work and pedaling rate. J. Biomech. 32, 1021-1026.

Nordeen-Snyder, K.S., 1977. The effect of bicycle seat height variation upon oxygen consumption and lower limb kinematics. Med. Sci. Sports Exerc. 9, 113-117.

Phinney, D., Carpenter, C., 1992. Training for cycling: the ultimate guide to improved performance. Putnam Publishing Group, NY, pp. 82.

Richmond, D.R., 1994. Handlebar problems in bicycling. Clin. Sports Med. 13, 165-173.

Sanderson, D.J., Black, A., 2003. The effect of prolonged cycling on pedal forces. J. Sports Sci. 21, 191-199.

Sangeorzan, B.J., Harrington, R.M., Wyss, C.R., Czerniecki, J.M., Matsen, F.A., 1989. Circulatory and mechanical response of skin to loading. J. Orth. Res. 7, 425-431.

Smak, W., Neptune, R.R., Hull, M.L., 1999. The influence of pedaling rate on bilateral asymmetry in cycling. J. Biomech. 32, 899-906.

Stone, C., Hull, M.L., 1995. The effect of rider weight on rider-induced loads during common cycling situations. J. Biomech. 28, 365-375.

Usabiaga, J., Crespo, R., Iza, I., Aramendi, J., Terrados, N., Poza, J.J., 1997. Adaptation of the lumbar spine to different positions in bicycle racing. Spine 22, 1965-1969.

Vuong, P.N., Camuzard, P., Schoonaert, M.F., 1988. Perineal nodular indurations ("accessory testicles") in cyclists. Acta Cytol. 32, 86-90.

Weiss, B.D., 1994. Clinical syndromes associated with bicycle seats. Clin. Sports Med. 13, 175-187.

Weiss, B.D., 1985. Nontraumatic injuries in amateur long distance bicyclists. Am. J. Sports Med. 13, 187-192.

